# SECOND-ORDER TURBULENT MODELING APPLIED TO MOMENTUMLESS WAKES IN STRATIFIED FLUIDS

W. Stephen Lewellen Milton Teske, et al

Aeronautical Research Associates of Princeton, Incorporated

Prepared for:

Defense Advanced Research Project Agency

November 1973

Sponsored by
Defense Advanced Research Projects Agency
DARPA Order No. 1910

# A.R.A.P. REPORT NO. 206

# SECOND-ORDER, TURBULENT MODELING APPLIED TO MOMENTUMLESS WAKES IN STRATIFIED FLUIDS



by
W. S. Lewellen, M. Teske and Coleman duP. Donaldson

This work was supported by the
Defense Advanced Research Projects Agency of the Department of Defense
and was monitored by the Office of Naval Research under
Contract N00014-72-C-0413



Aeronautical Research Associates of Princeton, Inc.
50 Washington Road, Princeton, New Jersey 08540
609-452-2950

November 1973

Security Classification

AD 771725

## DOCUMENT CONTROL DATA - R & D

*(Security classification of title, body of abstract and indexing annotation must be entered when the overall report is classified)*

1. ORIGINATING ACTIVITY (Corporate author)

Aeronautical Research Associates of Princeton
50 Washington Road, Princeton, N. J. 08540

2a. REPORT SECURITY CLASSIFICATION
Unclassified

2b. GROUP

3. REPORT TITLE

"Second-Order, Turbulent Modeling Applied to Momentumless Wakes in Stratified Fluids"

4. DESCRIPTIVE NOTES (Type of report and inclusive dates)
Interim

5. AUTHOR(S) (First name, middle initial, last name)

W. Stephen Lewellen
Coleman duP. Donaldson
Milton Teske

| 6. REPORT DATE | 7a. TOTAL NO. OF PAGES | 7b. NO. OF REFS |
|---|---|---|
| November 1973 | 47 | 18 |

8a. CONTRACT OR GRANT NO.
N00014-72-C-0413 new

b. PROJECT NO.
DARPA Order No. 1910

c.

d.

9a. ORIGINATOR'S REPORT NUMBER(S)
A.R.A.P. Report No. 206

9b. OTHER REPORT NO(S) (Any other numbers that may be assigned this report)

10. DISTRIBUTION STATEMENT

This document has been approved for public release and sale; its distribution is unlimited.

11. SUPPLEMENTARY NOTES

12. SPONSORING MILITARY ACTIVITY
Defense
Advanced Research Projects Agency

13. ABSTRACT

The technique of second-order closure for turbulence modeling is used to treat the growth and decay of turbulence, and the generation of internal waves behind a submarine moving at constant velocity through a stratified ocean. A computer model based on the solution of five partial differential equations and approximating nine others is generated. Required model coefficients are obtained by comparison with data obtained from laboratory flows and the atmospheric surface layer. The model is verified by comparison with Naudascher's wake data in the limit of vanishing stratification; with Wu's observations in the limit of starting with a uniformly mixed region in a strongly stratified fluid; and with Hartman and Lewis's analytical predictions in the limit of a small perturbation to the ambient linear density gradient and vanishing turbulence. Model runs are made demonstrating that the strength of the internal waves generated by a decaying wake increase with increasing initial potential energy (unless the initial Richardson number $Ri \ll 1$), or increasing initial kinetic energy (unless $Ri \gg 1$), or increasing ambient stratification gradient.



DD FORM 1 NOV 65 1473

Security Classification

| 14. KEY WORDS | LINK A | | LINK B | | LINK C | |
|---|---|---|---|---|---|---|
| | ROLE | WT | ROLE | WT | ROLE | WT |
| Submarine wakes | | | | | | |
| Turbulence modeling | | | | | | |
| Internal wave generation | | | | | | |
| Momentumless wakes | | | | | | |

## SUMMARY

A computational model has been developed for the turbulent wake of a submarine moving at a constant velocity through a stratified ocean. Details of the wake growth, collapse and generation of internal gravity waves were examined by an application of the second-order closure approach to turbulent flow developed at A.R.A.P. over the past few years. The empirical model coefficients required for basic imcompressible flow were determined by examining the distributions of turbulence in free jets and wall shear layers; the additional coefficients involving the influence of density stratification were found by comparison with observations in the atmospheric shear layer.

The model predictions agree with laboratory observations in both the limit of vanishing stratification and the opposite limit of a strongly stratified fluid with vanishing turbulence. Also in the limit of a small perturbation to the ambient density stratification and vanishing turbulence, the model results agree with analytic predictions of the internal gravity waves.

The influence of some of the major parameters has been demonstrated by running a few typical cases. Increasing the initial potential energy in the wake increases the strength of collapse unless the product of the Brunt-Väisälä frequency of the fluid times the characteristic dimension of the wake is much less than the characteristic turbulent velocity (i.e., $Ri_o \ll 1$), in which case there is no effect. Increasing the initial kinetic energy increases the strength of collapse unless $Ri_c \gg 1$, in which case there is no effect. Increasing the Brunt-Väisälä frequency of the fluid always appears to advance the time and increase the strength of collapse.

TABLE OF CONTENTS

## NOMENCLATURE

| | |
|---|---|
| $a, A, b$ | model constants |
| $C_D$ | drag coefficient of generating body |
| $D$ | diameter of generating body |
| $Fr$ | wake Froude number = $r_i N/U$ |
| $g$ | gravitational acceleration |
| $N$ | Brunt-Väisälä frequency = $[-(g/\rho)\ \partial\rho_o/\partial z]^{\frac{1}{2}}$ |
| $p$ | pressure |
| $q$ | square root of twice the turbulent kinetic energy |
| $r$ | wake radius |
| $r_i$ | initial wake radius |
| $Re$ | Reynolds number = $Ur_i/\nu$ |
| $Ri$ | Richardson number of turbulence = $r_i^2 N^2/q_m^2$ |
| $s$ | model constant |
| $u$ | velocity departure in free stream direction normalized by $U$ |
| $u_i, u_j, u_k$ | Cartesian velocity components |
| $U$ | free stream uniform velocity |
| $v$ | horizontal velocity normalized by $U$ |
| $v_c$ | model constant |
| $w$ | vertical velocity normalized by $U$ |
| $x_i, x_j, x_k$ | Cartesian coordinates |
| $x$ | coordinate in free stream direction |
| $y, z$ | coordinate in horizontal, vertical direction normalized by initial wake radius |
| $Y, Z$ | normalized plotting coordinate = $cy$, $cz$ ($c = 1.45$ in all figures except Fig. 3 and 6 where $c = 2.75$) |

| | |
|---|---|
| $\kappa$ | coefficient of laminar diffusion for density perturbation |
| $\lambda$ | microscale of turbulent dissipation |
| $\Lambda$ | macroscale of turbulent model |
| $\nu$ | kinematic viscosity |
| $\pi$ | perturbation pressure = $p + \int g\rho_o dz$ |
| $\rho$ | density |
| $\hat{\rho}$ | normalized perturbation density = $(\rho - \rho_o)/(r_1 \partial\rho_o/\partial z)$ |
| $\rho_o$ | ambient fluid density |
| $\psi$ | stream function = $\int v dz = -\int w dy$ |

superscripts

| | |
|---|---|
| $\overline{\quad}$ | denotes time average |
| ' | denotes fluctuation about the mean value |

subscript

| | |
|---|---|
| m | denotes maximum value |

# 1. INTRODUCTION

A submarine moving at constant speed through a stratified ocean leaves behind a turbulent wake containing potential and kinetic energy. The build-up of potential energy is caused by the co-mixing of heavier density fluid above the lighter density fluid. The kinetic energy is composed principally of the turbulent contribution. In the initial stages of the wake, the turbulent kinetic energy dominates the potential energy and the wake spreads. This spreading in turn increases the potential energy, until at some point gravitational forces are able to overcome the turbulence and force a collapse of the vertical spread of the wake.

The wake collapse has been studied both experimentally (Refs. 1-3) and theoretically (Refs. 4-10) to gain a qualitative understanding of the phenomenon. The theoretical studies have dealt primarily with idealized, inviscid collapse of an initially mixed region, the exception being Ko's analysis (Ref. 9) which attempts to include full coupling between the dynamics of the turbulence and the collapse, albeit in a simplified, integral approach.

The present analysis uses the techniques of second-order closure for turbulence modeling (Ref. 11) to treat the dynamic coupling between the turbulence and the stratification in some detail. We are concerned here with the growth and decay of the turbulence and the generation of internal waves, but not with the propagation of these waves to distances far outside the turbulent wake.

The turbulence model is discussed in Section 2. The computational scheme for dividing the wake into regions governed by different physical phenomena is discussed in Section 3. Numerical results are presented in Section 4.

## 2. THE TURBULENCE MODEL

The time-averaged equations of motion for a Boussinesq fluid whose motion consists of a mean and a fluctuating part may be written as

$$\frac{\partial u_i}{\partial x_i} = 0 \tag{1}$$

$$\frac{Du_i}{Dt} = -\frac{1}{\rho_o}\frac{\partial p}{\partial x_i} - \frac{\partial \overline{u_i' u_j'}}{\partial x_j} + \frac{\partial}{\partial x_j}\left(\nu \frac{\partial u_i}{\partial x_j}\right) - \frac{g_i \rho}{\rho_o} \tag{2}$$

Whether the density variation is caused by a temperature variation or a variation in composition, when the ambient density gradient is constant the diffusion equation for the perturbation density $\rho - \rho_o$ may be written as

$$\frac{D(\rho-\rho_o)}{Dt} = \frac{\partial}{\partial x_j}\left(\kappa \frac{\partial \rho - \rho_o}{\partial x_j}\right) - \frac{\partial \overline{u_j' \rho'}}{\partial x_j} - u_i \frac{\partial \rho_o}{\partial x_i} \tag{3}$$

Starting from the equations of motion for the fluctuating components of velocity and density, it is possible to derive exact equations for the Reynolds stress correlation $\overline{u_i' u_j'}$ and the correlations involving the $\rho'$ density fluctuation. These may be written as

$$\frac{D\overline{u_i' u_j'}}{Dt} = -\overline{u_i' u_k'}\frac{\partial \bar{u}_j}{\partial x_k} - \overline{u_j' u_k'}\frac{\partial \bar{u}_i}{\partial x_k} - \frac{g_i}{\rho_o}\overline{u_j' \rho'} - \frac{g_j \overline{u_i' \rho'}}{\rho_o} + \frac{\partial}{\partial x_k}\left(\overline{u_k' u_i' u_j'}\right)$$

$$- \frac{1}{\rho_o}\frac{\partial \overline{p' u_i'}}{\partial x_j} - \frac{1}{\rho_o}\frac{\partial \overline{p' u_j'}}{\partial x_i} + \overline{\frac{p'}{\rho_o}\left(\frac{\partial u_i'}{\partial x_j} + \frac{\partial u_j'}{\partial x_i}\right)} + \nu \frac{\partial^2 \overline{u_i' u_j'}}{\partial x_k^2}$$

$$- 2\nu \overline{\frac{\partial u_i'}{\partial x_k}\frac{\partial u_j'}{\partial x_k}} \tag{4}$$

$$\frac{D\overline{u_i'\rho'}}{Dt} = -\overline{u_i'u_j'}\frac{\partial\rho}{\partial x_j} - \overline{u_j'\rho'}\frac{\partial\bar{u}_i}{\partial x_j} - \frac{g_i}{\rho_o}\overline{\rho'^2} - \frac{1}{\rho_o}\frac{\partial}{\partial x_i}(\overline{p'\rho'})$$

$$+ \overline{\frac{p'}{\rho_o}\frac{\partial\rho'}{\partial x_i}} - \overline{\nu\rho'\frac{\partial^2 u_i'}{\partial x_j^2}} - \overline{\kappa u_i'\frac{\partial^2\rho'}{\partial x_j^2}} \qquad (5)$$

$$\frac{D\overline{\rho'^2}}{Dt} = -2\overline{u_j'\rho'}\frac{\partial\rho}{\partial x_j} - \frac{\partial}{\partial x_j}\overline{u_j'\rho'^2} - \overline{2\kappa\frac{\partial\rho'}{\partial x_j}\frac{\partial\rho'}{\partial x_j}} \qquad (6)$$

Second-order turbulence modeling involves deriving (or sometimes assuming) relationships between the third-order correlations appearing in Eqs. (4) - (6) and the derivatives of lower-order correlations. We choose to model the third-order correlations as (Ref. 11)

Dissipation terms:

$$2\nu\overline{\frac{\partial u_i'}{\partial x_k}\frac{\partial u_j'}{\partial x_k}} = 2\nu\left[\delta_{ij}\frac{q^2}{3\lambda^2} + \frac{a}{\Lambda^2}\left(\overline{u_i'u_j'} - \delta_{ij}\frac{q^2}{3}\right)\right] \qquad (7)$$

$$\overline{\nu\rho'\frac{\partial^2 u_i'}{\partial x_j^2}} + \overline{\kappa u_i'\frac{\partial^2\rho'}{\partial x_j^2}} = \frac{a}{\Lambda^2}(\nu + \kappa)\,\overline{u_i'\rho'} \qquad (8)$$

$$2\kappa\overline{\frac{\partial\rho'}{\partial x_j}\frac{\partial\rho'}{\partial x_j}} = 2\kappa s\frac{\overline{\rho'^2}}{\lambda^2} \qquad (9)$$

with

$$\lambda^2 = \frac{\Lambda^2}{(a + b\Lambda q/\nu)}$$

Pressure strain terms:

$$\overline{\frac{p'}{\rho}\left(\frac{\partial u_i'}{\partial x_j} + \frac{\partial u_j'}{\partial x_i}\right)} = - \frac{q}{\Lambda}\left(\overline{u_i'u_j'} - \frac{\delta_{ij}}{3} q^2\right) \tag{10}$$

$$\overline{\frac{p'}{\rho_o}\frac{\partial \rho'}{\partial x_i}} = - A \frac{q}{\Lambda} \overline{u_i'\rho'} \tag{11}$$

Diffusion terms:

$$\overline{u_k'u_i'u_j'} = - v_c q \Lambda \left( \frac{\partial \overline{u_i'u_k'}}{\partial x_j} + \frac{\partial \overline{u_k'u_j'}}{\partial x_i} + \frac{\partial \overline{u_i'u_j'}}{\partial x_k} \right) \tag{12}$$

$$\overline{\frac{p'}{\rho_o} u_i'} = v_c q \Lambda \frac{\partial \overline{u_i'u_k'}}{\partial x_k} \tag{13}$$

$$\overline{u_i'u_j'\rho'} = - v_c q \Lambda \frac{\partial \overline{u_i'\rho'}}{\partial x_j} \tag{14}$$

$$\overline{u_j'\rho'^2} = - v_c q \Lambda \frac{\partial \overline{\rho'^2}}{\partial x_j} \tag{15}$$

$$\overline{\frac{p'\rho'}{\rho_o}} = v_c q \Lambda \frac{\partial}{\partial x_i} \overline{u_i'\rho'} \tag{16}$$

Reasonable values for the coefficients a, b , and $v_c$ were determined in Refs. 11 and 12 as 2.5, 0.125 and 0.3, respectively, by examining the turbulent distributions in free jets and wall shear layers. The coefficients A and s which influence the effect of stratification were assigned the values of 0.75 and 1.8, respectively, in Ref. 13 to obtain good agreement with the turbulence distributions observed in the atmospheric surface layer. With this choice of model coefficients, model predictions for the mean velocity gradient, mean temperature gradient, Richardson number, rms vertical velocity

fluctuations, rms temperature fluctuations and horizontal heat flux agreed favorably with surface layer experimental observations over the complete range of stability conditions. The values cited above for the coefficient, $a$, $b$, $v_c$, $A$ and $s$ will be used in the present analysis.

Equations (1) through (6) represent a formidable set for the general three-dimensional wake. To keep the problem manageable for our relatively small computer (a Digital Scientific Corp. META-4), we have simplified the equations in certain regions of the downstream development of the wake. Our approximation consists of neglecting the convective and diffusion terms in the equations obtained by substituting Eqs. (7) through (16) into (4) through (6) to form a set of algebraic relationships between the turbulent correlations and the mean flow derivatives, but retaining convection and diffusion of the turbulence by carrying the equation for $q^2 = \overline{u_i' u_i'}$. Equations (4) through (6) are replaced by

$$\frac{Dq^2}{Dt} = -2\,\overline{u_i'u_j'}\,\frac{\partial \bar{u}_i}{\partial x_j} - 2\,\frac{g_i}{\rho_o}\,\overline{u_i'\rho'} + \frac{\partial}{\partial x_i}\left[(q\Lambda + \nu)\,\frac{\partial q^2}{\partial x_i}\right] - \frac{2\nu q^2}{\lambda^2} \tag{17}$$

$$0 = -\overline{u_i'u_k'}\,\frac{\partial \bar{u}_j}{\partial x_k} - \overline{u_j'u_k'}\,\frac{\partial \bar{u}_i}{\partial x_k} - g_i\,\frac{\overline{u_j'\rho'}}{\rho_o} - g_j\,\frac{\overline{u_i'\rho'}}{\rho_o}$$

$$- \frac{q}{\Lambda}\left(\overline{u_i'u_j'} - \frac{q^2}{3}\,\delta_{ij}\right) - 2(b - f)\,\frac{q^3}{3\Lambda}\,\delta_{ij} \tag{18}$$

$$0 = -\overline{u_i'u_j'}\,\frac{\partial \rho}{\partial x_j} - \overline{u_j'\rho'}\,\frac{\partial \bar{u}_i}{\partial x_j} - g_i\,\frac{\overline{\rho'^2}}{\rho_o} - \frac{Aq}{\Lambda}\,\overline{u_i'\rho'} \tag{19}$$

$$0 = -2\,\overline{u_j'\rho'}\,\frac{\partial \rho}{\partial x_j} - 2sbq\,\frac{\overline{\rho'^2}}{\Lambda} \tag{20}$$

Note that the function $f$ has been added to Eq. (18) to allow Eq. (17) to be added without making the system overdetermined. The term is added in such a way that the influence of the convective and diffusion terms in Eq. (17) are distributed equally between the three components of $q^2$. Also, the diffusion term in Eq. (17) is somewhat simplified from that which would be obtained for $\overline{u_i'u_i'}$ from Eq. (4).

The set of equations (1), (2), (3), (17), (18), (19) and (20) make up what we will call the quasi-equilibrium (QE) approximation for second-order closure. It is closely related to what Mellor and Herring (Ref. 14) refer to as mean turbulent energy closure. It reduces to the same number of differential equations but retains more of the coupling between the components of the Reynolds stress through the algebraic relations, Eqs. (18) - (20).

Figure 1 gives a comparison of the QE results with that for the full set for the case of an unstratified, axisymmetric wake. Results for the full set are taken from Ref. 12 from an axisymmetric calculation while the QE results are taken from a 3-D, stratified calculation in the limit of negligible stratification. The $q^2$ distributions agree quite closely while the mean velocity departure from free stream shows about a 10% difference when it has been allowed to decay an order of magnitude from the initial conditions. The great simplification made possible by the QE approximation appears to be ample justification for this slight loss in accuracy. Comparisons of the two methods have also been made in calculations of the planetary boundary layer which show relatively little difference between the two, but these results will not be shown here.

The scale length $\Lambda$ in Eqs. (17) - (20) should in fact be solved by its own differential equation, enabling us to determine the $\Lambda$ variation across the wake as the solution proceeds downstream. The equation for $\Lambda$ would be similar to the equation for $q^2$, Eq. (17). We choose not to do this, however, since the scale equation has not yet become an integral part of the second-order turbulence model we

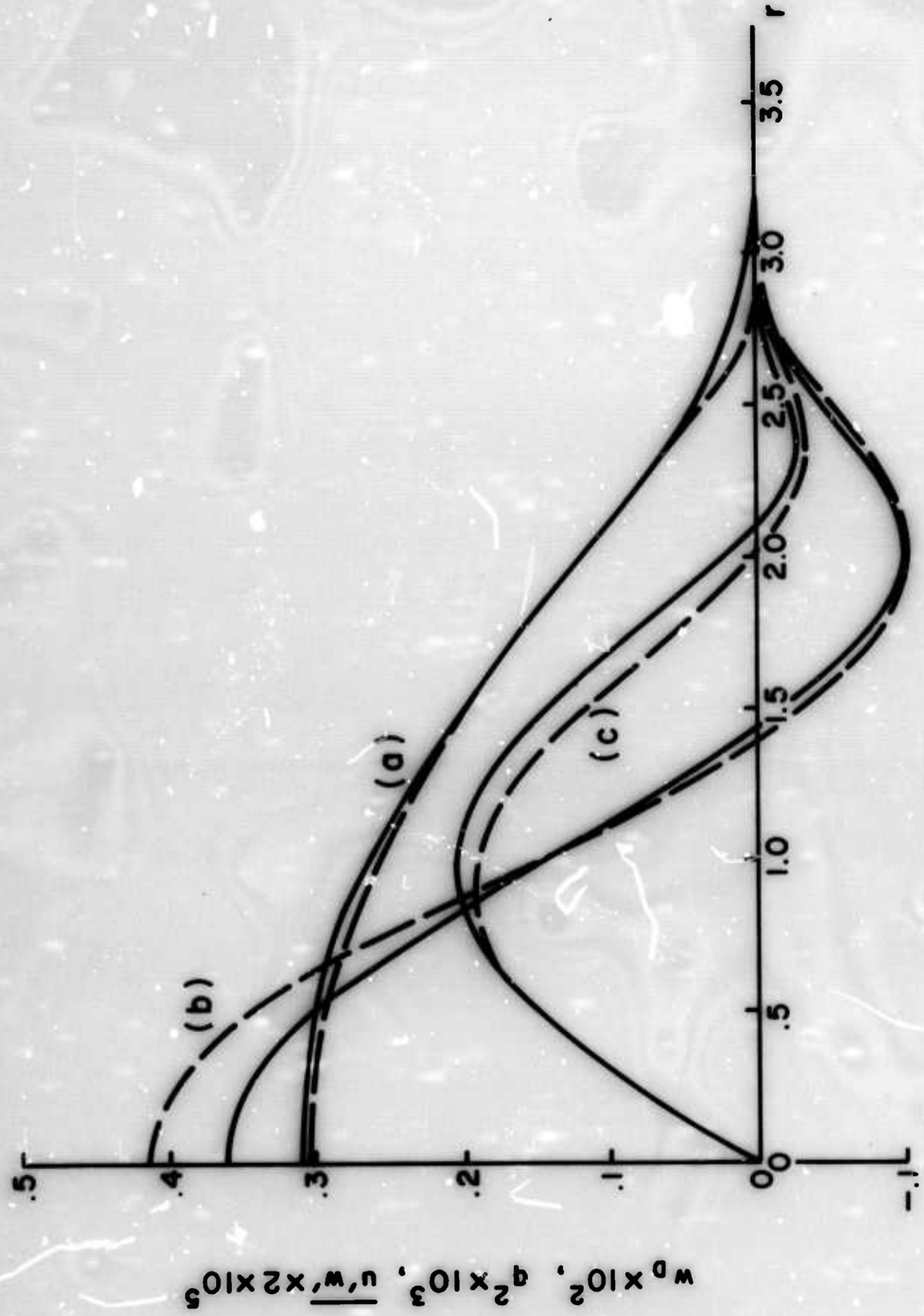


Figure 1. Comparison of quasi-equilibrium results (---) with results from the full equations (——). Distributions are shown at the same station (x/D=100) after starting with identical conditions (@ x/D = 20) a) turbulent energy $q^2$, b) mean velocity departure from freestream $w_D$, and c) shear stress $\overline{u'w'}$.

are using. Instead, we choose to use a $\Lambda$ geared to the breadth of the $q^2$ turbulent wake region. For our analysis here and in the free jet examination (Ref. 12), we assume that $\Lambda$ is proportional to the distance from the radius of the maximum $q^2$ (typically $r = 0$) out to the radius where the value of $q^2$ has dropped to 1/4 its maximum value. Comparison with the axisymmetric flows in the near-wake region yield a proportionality factor of 0.2.

The $\Lambda$ that results from this algebraic relationship now expands or collapses depending upon the turbulence within the wake. Since, when collapse occurs, the scale in the vertical $z$ direction can be greatly distorted from the horizontal $y$ scale, we have chosen to compute separate scales along the $y$ and $z$ axes. These resulting $\Lambda_y$'s and $\Lambda_z$'s then go directly into their appropriate diffusion terms in the $q^2$ equation. The QE approximation and the dissipation term $-2bq^3/\Lambda$ use only one scale length. Since we anticipate that the collapse will yield an ellipse-like wake region, we have chosen the equation for $\Lambda$ as

$$\Lambda = \frac{2\Lambda_y^2 \Lambda_z}{\Lambda_y^2 + \Lambda_z^2}$$

Thus, when $\Lambda_y >> \Lambda_z$ for complete collapse, $\Lambda \rightarrow 2\Lambda_z$ and enables $\Lambda$ to track the details of the vertical collapse. Following Ref. 13 we also impose an upper limit on the vertical scale

$$\Lambda_{z_{max}} = \left( \frac{Ri^* \, q_m^2}{-\frac{g}{\rho_o} \frac{\partial \rho}{\partial z}} \right)^{\frac{1}{2}}$$

where $Ri^*$ is a critical Richardson number found from the atmospheric surface layer to be $Ri^* = 0.25$.

## 3. COMPUTATIONAL SCHEME

A typical turbulent wake in a stratified medium can be divided into regions governed by different physical phenomena. At the aft end of the body, the flow is dominated by the details of the body shape and mode of propulsion (this problem will not be discussed here). A short distance downstream of the body in the near wake, the kinetic energy of the mean flow is converted into turbulent kinetic energy. As long as the potential energy in the near wake is much smaller than the kinetic energy, which should be true as long as

$$- r_i^4 g \frac{\partial \rho_o}{\partial z} \ll C_D r_i^2 \rho U^2 \tag{21}$$

i.e.,

$$- \frac{r_i^2 g}{U^2 \rho} \frac{\partial \rho_o}{\partial z} = F_r^{-2} \ll C_D \tag{22}$$

it should be possible to ignore the effect of stratification in this region. Thus if there are no asymmetries introduced by the body, the near wake may be treated as an axisymmetric flow. Equations (2) and (4) were integrated for unstratified, axisymmetric flow in Ref. 12. The model demonstrated the strong influence of net mean momentum on the development of the wake, with the model predictions verified by comparisons with existing data for a wake behind a self-propelled body and for a wake with significant mean momentum.

The near-wake region should remain valid as long as the turbulence is strong enough to dominate the stratification, i.e., as long as

$$- \frac{r_i^2 g}{q_m^2 \rho} \frac{\partial \rho_o}{\partial z} = Ri \ll 1 \tag{23}$$

Although the stratification does not influence the turbulence significantly in the near-wake region, the density distribution is determined by the turbulence. Thus, for stratified flow it is necessary to carry the additional Eqs. (3), (5) and (6). However, as long as the initial conditions contain only the streaming velocity, it is possible to reduce Eq. (2) to a scalar equation for $u$. Assuming that diffusion in the free stream direction is negligible compared with that normal to the free stream, that the pressure gradient in the free stream direction is zero, and that the mean flow departure from the free stream is small, we can reduce Eqs. (2) and (3) to:

$$\frac{\partial u}{\partial x} = \frac{1}{Re} \nabla^2 u - \frac{\partial \overline{u'w'}}{\partial z} - \frac{\partial \overline{u'v'}}{\partial y} \tag{25}$$

$$\frac{\partial \hat{\rho}}{\partial x} = \frac{Pr}{Re} \nabla^2 \hat{\rho} - \frac{\partial \overline{w'\rho'}}{\partial z} - \frac{\partial \overline{v'\rho'}}{\partial y} \tag{26}$$

where

$$\nabla^2 = \frac{\partial^2}{\partial y^2} + \frac{\partial^2}{\partial z^2}$$

If we accept the quasi-equilibrium approximation for the turbulence discussed in the last section, then the set is completed by taking

$$\frac{\partial q^2}{\partial x} = -\frac{2}{Fr^2} \overline{w'\rho'} - 2\,\overline{u'v'}\,\frac{\partial u}{\partial y} - 2\,\overline{u'w'}\,\frac{\partial u}{\partial z}$$

$$+ \frac{\partial}{\partial y}\left[\left(3v_c \frac{\overline{v'v'}}{q} \Lambda_y + \frac{1}{Re}\right)\frac{\partial q^2}{\partial y}\right]$$

$$+ \frac{\partial}{\partial z}\left[\left(3v_c \frac{\overline{w'w'}}{q} \Lambda_z + \frac{1}{Re}\right)\frac{\partial q^2}{\partial z}\right] - \frac{2q^2}{Re\lambda^2} \tag{27}$$

together with the algebraic relations given in Eqs. (8) - (20). In these equations, lengths have been normalized with respect to the initial wake radius $r_i$ ; velocities with the free stream velocity, $U$ ; and the perturbation density with $-r_i \partial\rho_o/\partial z$ . The dimensionless parameters are defined as $Re = U r_i/\nu$ , a Reynolds number; $Fr = [(-gr_i^2 \partial\rho_o/\partial z)/\rho U^2]^{-\frac{1}{2}}$ , a Froude number; and $Pr = \kappa/\nu$ , the Prandtl number. The algebraic relations between the second-order correlations bring in no additional parameters so the variables are a function only of Re, Pr and Fr plus the initial conditions on $q$ , $u$ , and $\hat{\rho}$ . The diffusion terms in the turbulent energy equation have been permitted to be more anisotropic in Eq. (27) than the form in Eq. (17). This form permits a larger influence of the stratification, but we have not been able to firmly establish which form is more accurate yet.

Equations (25) to (27) cease to be a valid approximation for the wake when the potential energy due to the perturbed density increases to the point where it is the same order of magnitude as the kinetic energy of the turbulence, i.e., when $Ri \gtrsim 0.1$ . Then the effect of the induced vertical velocity on the convection terms can no longer be neglected. To continue the wake calculations into the collapse region, it is then necessary to include the two transverse momentum equations from Eq. (2).

In the case of a momentumless wake, the mean velocity departure from free stream decays much more rapidly then the rms turbulent velocity so that with density stratification typical of the ocean (Brunt-Väisälä period of the order of one-half hour) the mean velocity departure becomes negligible before Ri reaches 0.1. Therefore, for many cases of interest we can set $u = 0$ and drop the axial momentum equation in the collapse region. The set of equations to be solved in this region within the quasi-equilibrium approximation now becomes

$$\frac{Dw}{Dt} = -\frac{\partial \pi}{\partial z} + \frac{1}{Re}\nabla^2 w - \frac{\partial \overline{v'w'}}{\partial y} - \frac{\partial \overline{w'w'}}{\partial z} - \frac{\hat{\rho}}{Fr^2} \tag{28}$$

$$\frac{Dv}{Dt} = -\frac{\partial \pi}{\partial y} + \frac{1}{Re}\nabla^2 v - \frac{\partial \overline{v'w'}}{\partial z} - \frac{\partial \overline{v'v'}}{\partial y} \tag{29}$$

$$\frac{D\hat{\rho}}{Dt} = +\frac{Pr}{Re}\nabla^2\hat{\rho} - \frac{\partial \overline{v'\rho'}}{\partial y} - \frac{\partial \overline{w'\rho'}}{\partial z} + w \tag{30}$$

$$\frac{Dq^2}{Dt} = -\frac{2}{Fr^2}\overline{w'\rho'} - \frac{2q^2}{Re\lambda^2} + \frac{\partial}{\partial y}\left[\left(3v_c\frac{\overline{v'v'}}{q}\Lambda_y + \frac{1}{Re}\right)\frac{\partial q^2}{\partial y}\right]$$

$$+ \frac{\partial}{\partial z}\left[\left(3v_c\frac{\overline{w'w'}}{q}\Lambda_z + \frac{1}{Re}\right)\frac{\partial q^2}{\partial z}\right] \tag{31}$$

$$\nabla^2\pi = -\frac{1}{Fr^2}\frac{\partial\hat{\rho}}{\partial z} - \frac{\partial^2\overline{v'v'}}{\partial y^2} - \frac{\partial^2\overline{w'w'}}{\partial z^2} - 2\frac{\partial^2\overline{v'w'}}{\partial y\partial z} + 2\frac{\partial v}{\partial y}\frac{\partial w}{\partial z}$$

$$- 2\frac{\partial v}{\partial z}\frac{\partial w}{\partial y} - \frac{\partial}{\partial x}\left[\frac{\partial v}{\partial y} + \frac{\partial w}{\partial z}\right] \tag{32}$$

The set is completed with the algebraic relationships for the correlations, Eqs. (18) to (20). Note that rather than work directly with the continuity equations, Eq. (1), we have taken the divergence of the momentum equation to obtain a Poisson equation for the perturbation pressure, $\pi = p + \int g\rho_o\,dz$. The last term in Eq. (32) has been retained because previous researchers found it desirable to correct for the fact that, numerically, Eq. (1) cannot be satisfied exactly.

In summarizing the division of the stratified wake development into a growth Phase (I) governed by Eqs. (25) - (27) and a collapse Phase (II) governed by Eqs. (28) - (32), we can say that (I) should hold as long as $Ri \lesssim 0.1$ while (II) should hold when $|u_m|/q_m \lesssim 0.1$ .

In the overlap region, which should occur as long as Ri immediately behind the body is sufficiently small, either set of equations may be used. If there is no overlap, such as may occur in the wake behind a low drag body moving slowly through a steep stratification, then our present computational scheme is not valid. Future modifications to our computer model will provide for the simultaneous solution of all three momentum equations so that this more general case can be analyzed. Figure 2 gives a comparison between the results of a Phase (I) and (II) computation for a case with a large overlap region. No significant differences are observed in the two solutions until after Ri = 0.07 at .04 B.V. (Brunt-Väisälä periods) after wake generation. Of course, Phase (I) represents a much more efficient computational scheme in the overlap region.

We have all of the information needed to solve the equations of interest for our Phase (I) or (II) regions. We begin our calculations in the near-wake region by assuming initial conditions for the turbulence, the perturbation density and mean $u$ profile. The Phase (I) region is permitted to build to the overlap region, at which time we introduce the normal velocities $v$ and $w$ and the pressure $\pi$ to proceed through the collapse Phase (II). To reduce redundant calculations, we consider only a quarter-plane of the wake cross-section, thus requiring us to impose appropriate symmetry conditions along both axes.

Since our primary purpose is to calculate the wake dynamics rather than the full wave pattern between the wake and the surface, we impose an artificial porous liner a few radii from the turbulent wake; this liner serves to absorb any waves emitted from the wake without reflecting them back to the wake. In this way we are justified in requiring all the variables $\to 0$ as $r \to \infty$. This absorption of the waves is implemented by adding the damping terms $-kw$ and $-kv$ to the right-hand sides of Eqs. (28) and (29), respectively, and the term $-v\,\partial k/\partial y - w\,\partial k/\partial z$ to the pressure Eq. (32). The damping factor $k$ is zero

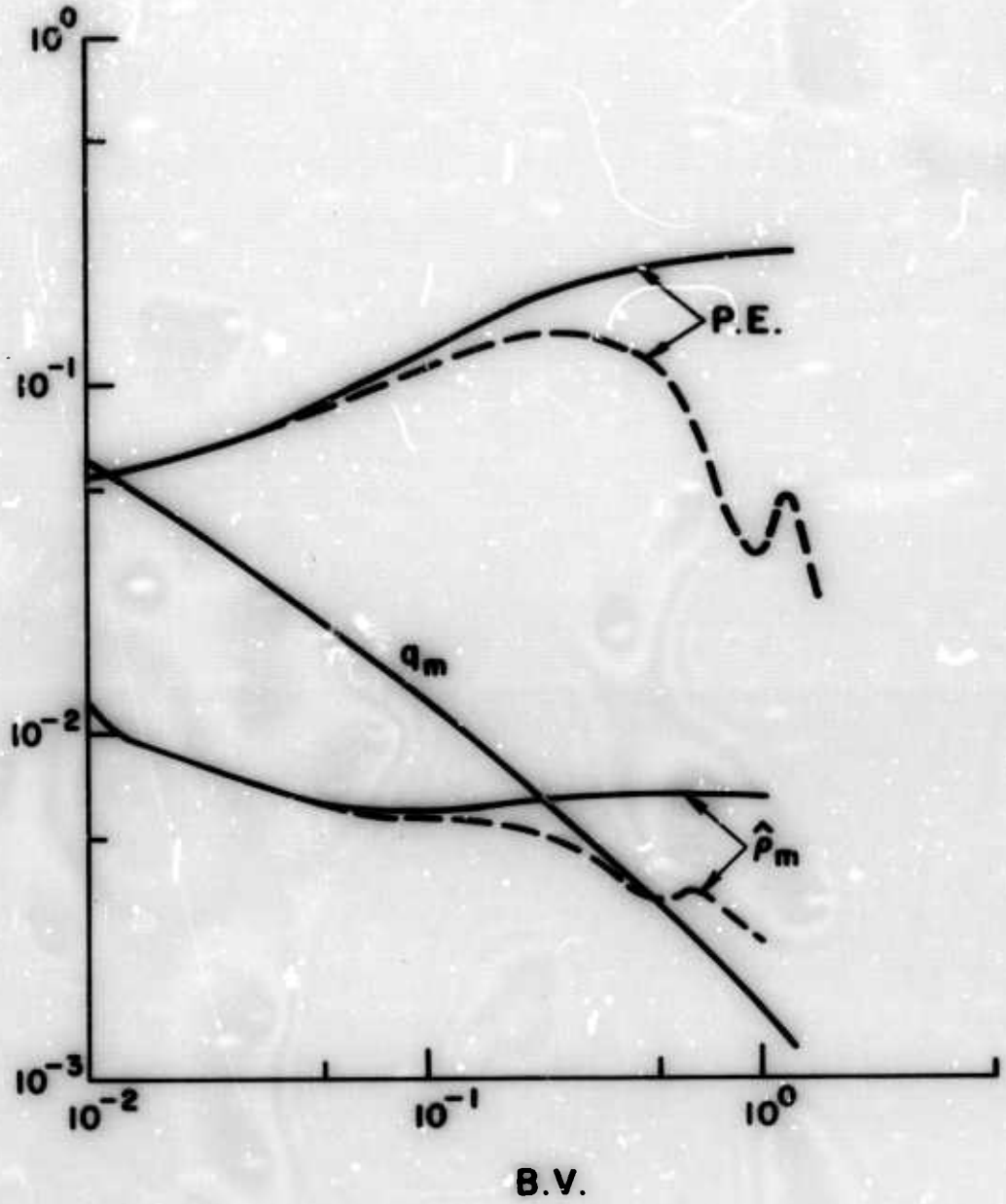


Figure 2. Comparison of Phase (I) and (II) calculations. (Initial conditions - Fr = 228., $q_m^2$ = .00456, $u_m$ = .00286, $\hat{\rho}_m$ = 1., v = w = 0.)

P.E. = $\int_{-\infty}^{+\infty}\int_{-\infty}^{+\infty} g(\rho-\rho_o)Z\,dYdZ$ .

out to a few wake radii and then increases smoothly to absorb any waves. As the wake dimension grows, the position of the liner also moves out at a proportional rate.

Figure 3 is a plot of density contours for two different positions of the absorbing liner. Although the contours are quite different outside the inner liner, there is little difference in the region of interest around the turbulent portion of the wake itself. A detailed comparison of these two cases shows that the average numerical difference at the points inside the inner liner is less than 5% of the maximum local value.

The differential equations discussed above are solved numerically by replacing them with forward-time-centered-space finite difference equations (Ref. 17). Since the equations involve two space directions $y$ and $z$ and a time-like direction $x$, we choose to solve them by the Alternating Direction Implicit (ADI) method (Ref. 18). The implicit technique permits stable solution development with a controlled increase in $\Delta x$ per step. The mesh in the $y$ and $z$ directions is variable, with mesh spacing $\Delta y$ and $\Delta z$ minimizing curvature changes from point to point.

When needed, the Poisson equation (Eq. (32)) for the perturbation pressure $\pi$ is solved by adding a time-like term $-\partial\pi/\partial t$ to the left-hand side of Eq. (32) and iterating by the ADI method to a steady state solution (so that $\partial\pi/\partial t \approx 0$) for every step in $q^2$, $\hat{\rho}$, $v$ and $w$. For the first two iteration steps, $\Delta t$ is given a value proportional to the area of the wake ($\Delta t = y_{max}\, z_{max}/40$) and allowed to increase or decrease thereafter at a rate determined internally in such a way as to try to maintain a change of $\approx 10\%$ with each iteration.

In practise our solution scheme takes a step $\Delta x$ in the main variables ($q^2$, $\hat{\rho}$, and $u$, or $v$ and $w$ as the case dictates), then the pressure is iterated for these new values. We find that our procedure works very well for Phase (I) (where no pressure iteration is required), but the Phase (II) pressure solution has

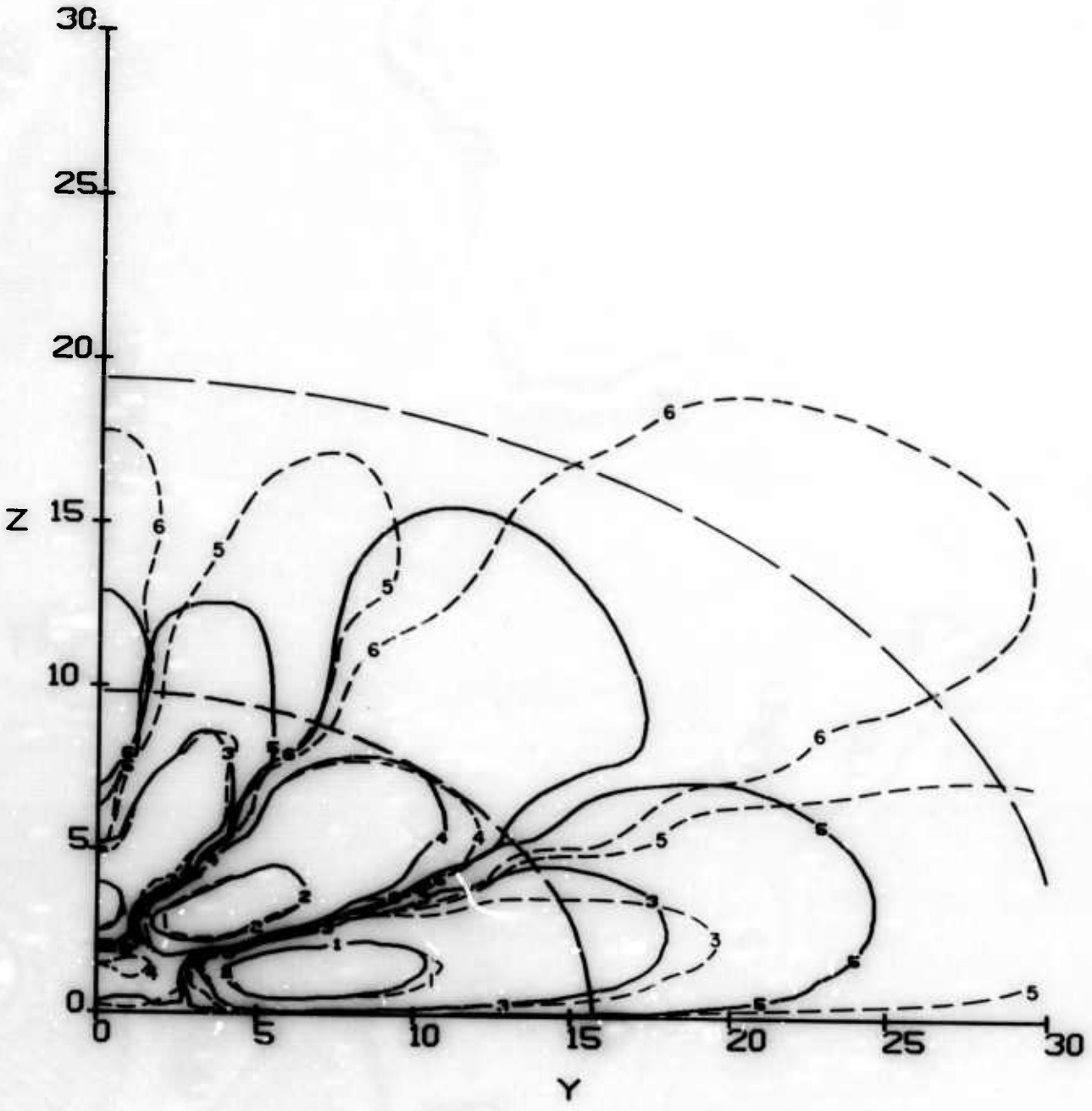


Figure 3. Comparison of density contours at one B.V. after wake generation for two positions of the porous liner. Outside the indicated dashed line the liner resistance increases from zero exponentially. --- contours for the case of the larger liner. (Initial conditions - Fr = 1.15, $q_m = u_m = v = w = 0$, $\hat{\rho}_m = 1.$) $\hat{\rho}_m = .280$ with contour for $\hat{\rho}/\hat{\rho}_m = +.5$ denoted by -1-; -.5 by -2-; +.1 by -3-; -.1 by -4-; +.01 by -5-; and -.01 by -6-.

caused the bulk of our numerical problems. It seems that our ADI method is not an extremely viable one when steady state is sought for $\pi$ at <u>every</u> step $\Delta x$. Rather, we found that stability and convergence were better controlled by limiting the number of pressure iterations at each step; a maximum of five iterations were permitted. This serves to keep the pressure close to an accurate value, and in turn keep $v$ and $w$, thus $\hat{\rho}$, accurate also. We monitor our accuracy by trying to keep the relative error

$$\epsilon_\pi = \frac{1}{\Delta t}\left[\frac{\int (\Delta\pi)^2 dy\, dz}{\int F^2 dy\, dz}\right]^{\frac{1}{2}} < 0.001$$

where $\Delta\pi$ is the change in $\pi$ in the step $\Delta t$, and $F$ is the value of the right-hand side of Eq. (32). $F$ has also been slightly modified by realizing that the term of most importance $-1/F_r^2\ \partial\hat{\rho}/\partial z$ can be estimated for the <u>next</u> step size $\Delta x$ and the pressure estimated ahead accordingly. Since the numerical technique is not exactly divergence free, the extra term on the right side of Eq. (32) in the form $\partial\nabla\cdot\bar{v}/\partial x$ is retained to make $\nabla\cdot\bar{v} = 0$ at the future $\Delta x$ main step.

A typical run in Phase (I) takes about 3 hours on the Digital Scientific META-4 (12 min. on CDC 6600), while Phase (II) takes about 12 hours on the META-4 (50 min. on CDC 6600) of which about 50% of the time is involved in the pressure iteration loop.

# 4. NUMERICAL RESULTS

Considerable confidence in our turbulence model was gained by the comparisons with the unstratified wakes in Ref. 12 and with the stratified atmospheric shear layer in Ref. 13. To gain some confidence in our computer model's capability to predict the generation of internal waves, we made a check with Hartman and Lewis's linear, inviscid solution (Ref. 5). Within our self-imposed limit of 40 x 40 mesh points, we were unable to maintain good agreement in the immediate neighborhood of the discontinuity at the edge of the homogeneously mixed region. However, results within the center of the mixed region agree with the exact solution to times greater than one B.V. Figure 4 is a comparison of the model results with the linear analytical predictions for radii less than 80% of the radius at which the discontinuity occurs. The bars on the model results give the r.m.s. deviation of the value at individual points about their mean.

Another check on the model is given in Fig. 5 by comparing with the experimental results of Wu (Ref. 3). Wu used a mechanical mixer to produce a cylindrical region of homogeneously mixed fluid surrounded by a strongly stratified fluid. His observations of the width of the mixed region as a function of time after release are plotted as given in Ref. 10. The model prediction for growth of the wake width for a case with large initial Ri and an initial homogeneously mixed wake is given as the solid curve. The agreement is similar to that obtained by the numerical models of Refs. 6 and 10. The streamline patterns predicted for this two-dimensional flow at times of 0.5, 1.0 and 1.5 B.V. after release are presented in Fig. 6. At earlier times there is only one vortex in the quadrant but other modes appear as time progresses. At t = 1.0 B.V. there are three distinct vortices, while at 1.5 B.V. two of these of the same sign have joined and a fourth is forming along the vertical axis.

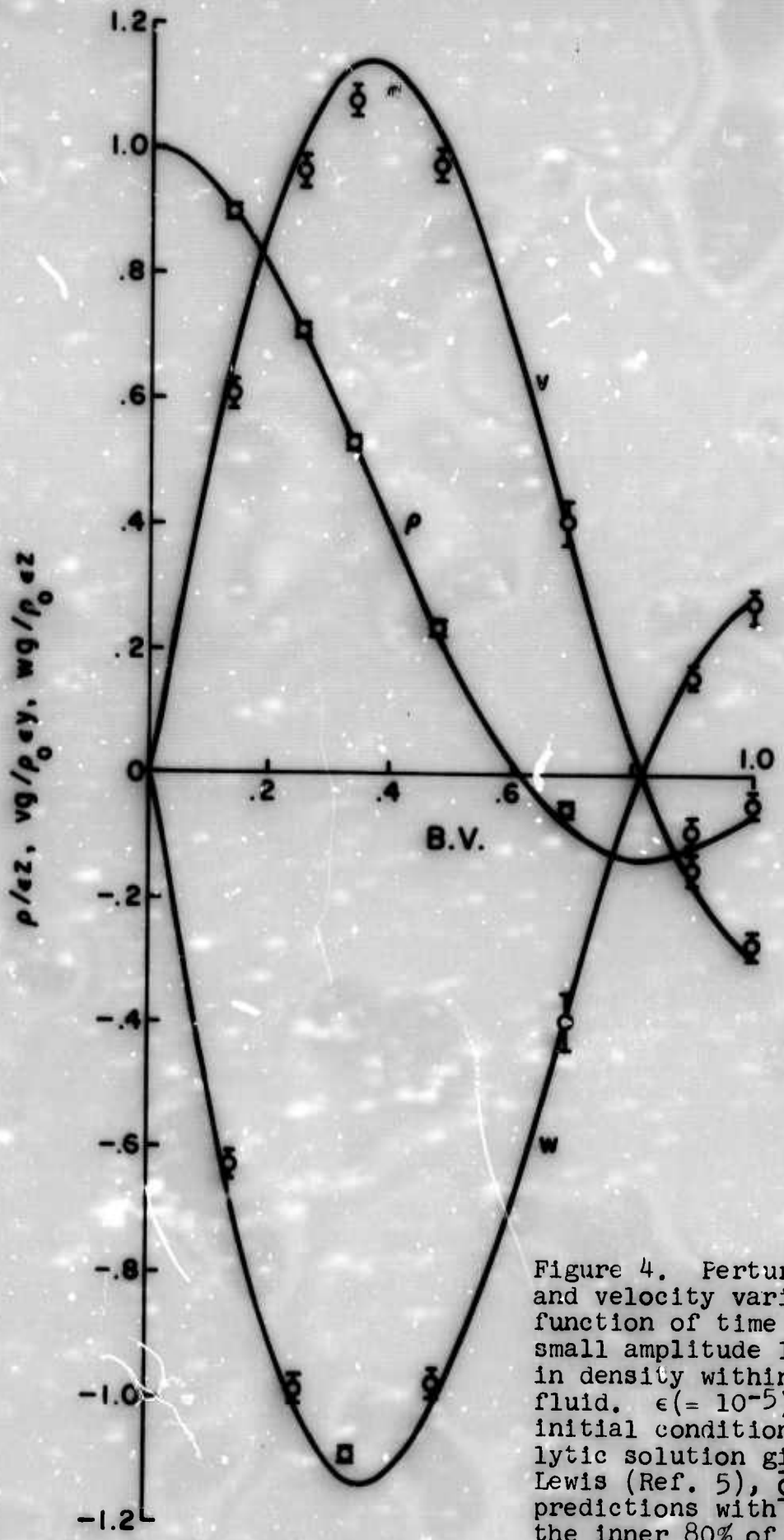


Figure 4. Perturbation density and velocity variations as a function of time for an inviscid, small amplitude linear perturbation in density within a cylinder of fluid. $\epsilon(= 10^{-5})$ defined by initial condition on $\hat{\rho}$ . —— analytic solution given by Hartman and Lewis (Ref. 5), $\bar{\Phi}$ numerical model predictions with r.m.s. scatter in the inner 80% of the radius of the cylinder as indicated.

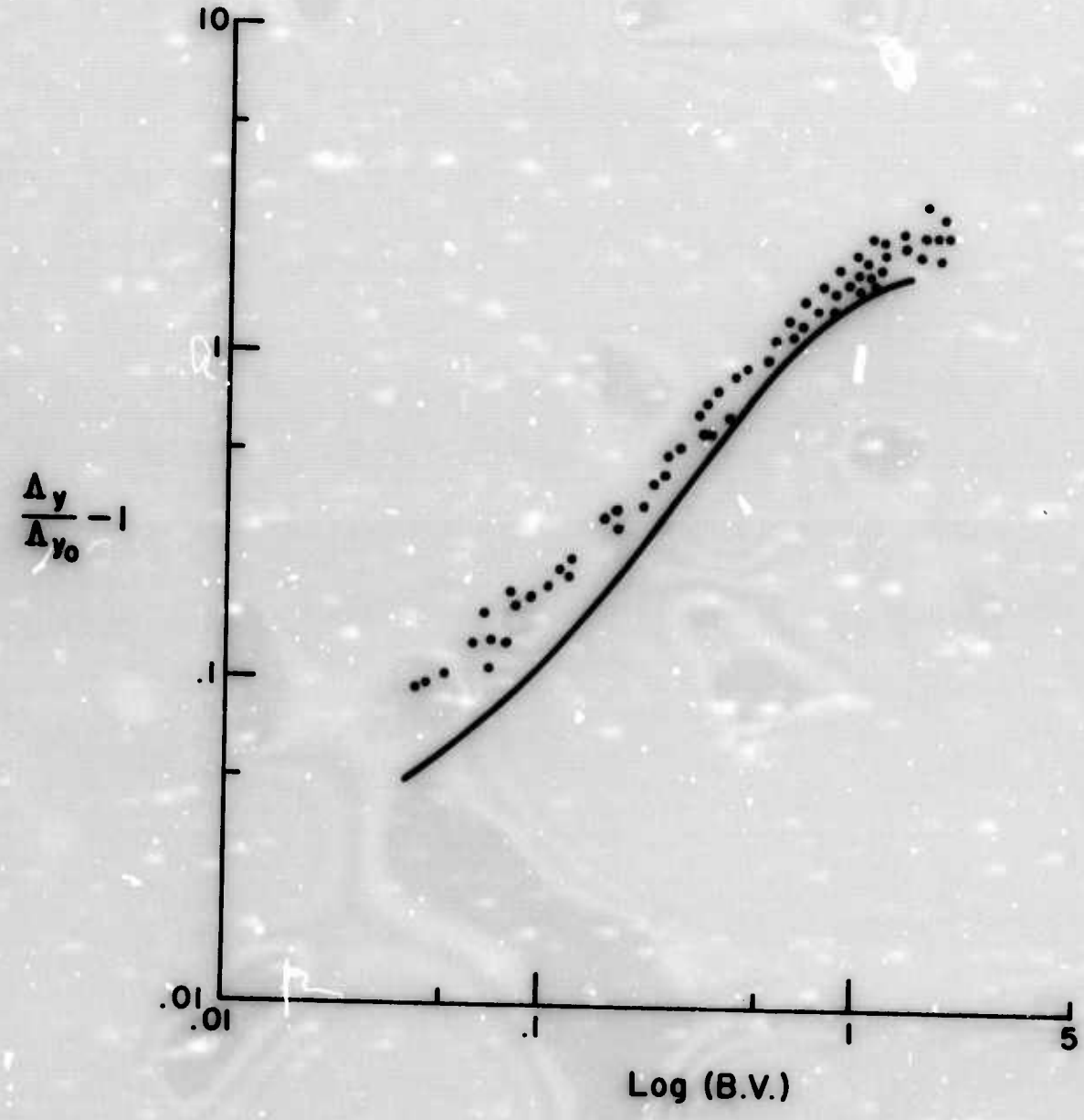


Figure 5. Horizontal wake spread as a function of time after generation. (Initial conditions - Fr = 1.15, $q_m = u_m = v = w = 0$, $\hat{\rho}_m = 1.$) —— model predictions, •.• experimental observations of Wu (Ref. 3).

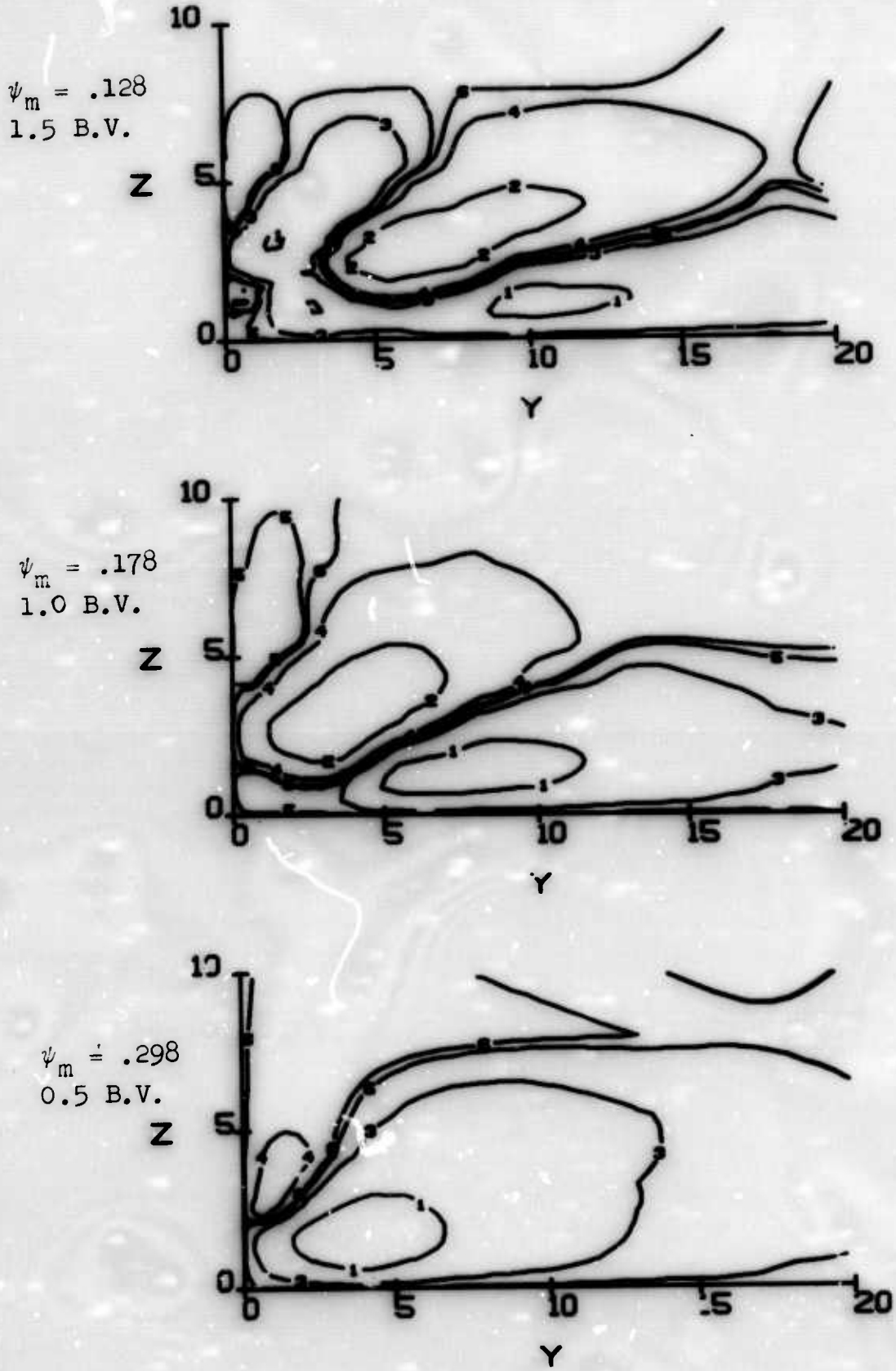


Figure 6. Streamline patterns for the same conditions as Fig. 5. Contours for $\psi/\psi_m$ as denoted in Fig. 3.

For our case of a momentumless wake the principal parameters are the Froude number $Fr = [-(g/\rho)\,\partial\rho_o/\partial z]^{-\frac{1}{2}}U/D$, the initial level of turbulence $q_m/U$, the initial density profile in the wake, and the Reynolds number of the turbulence $(q\,\Lambda/\nu)_{init}$. For a submarine wake the most important single parameter is a combination of the first two, a Richardson number for the stratified turbulent wake (Eq. (23)). As seen in the previous section when $Ri \ll 1$ right behind the body, the wake will grow for some distance behind the body before the wake collapses. Then the initial density distribution is relatively unimportant since the turbulent entrainment of fluid in the growth region will lead to a density distribution at the point where collapse begins which is independent of the initial distribution. The Reynolds number is not influential as long as it is large enough so that $q\Lambda/\nu$ remains much larger than one through the initial collapse. The only parameter we will consider in detail herein is Ri.

If Naudascher's (Ref. 15) values for turbulent intensities behind a self-propelled body are used as a starting point (although Gran (Ref. 16) indicates that his values are about a factor of two higher than would be obtained behind a streamlined body driven by an efficient propeller), then a body with a radius of five meters moving through a stratified fluid with $N^2 = 10^{-5}/\text{sec}^{-2}$ at a velocity of five meters/sec would have $Ri \approx 10^{-2}$ at a station 20 diameters downstream of the body. Figure 7 is a plot of some of the wake variables as a function of distance downstream of the body or, equivalently, time after generation for a run in which we start with a homogeneously mixed density and Naudascher's values of turbulence at $x/D = 20$. Up to $x/D \approx 200$ where $Ri \approx 1$, the results for $q$ are the same as obtained in Ref. 12 for an unstratified wake; the density perturbation is being reduced as the wake entrains more fluid; and $v$ and $w$ are much less than $q$. At larger distances downstream there is a significant difference in the shape of the wake although the maximum $q$ shows little difference. Although $v$ and $w$ build to maximum velocities at approximately 0.5 B.V., they remain smaller than $q$. Figures 8, 9 and 10 show the contours of $\hat{\rho}$ and $q^2$

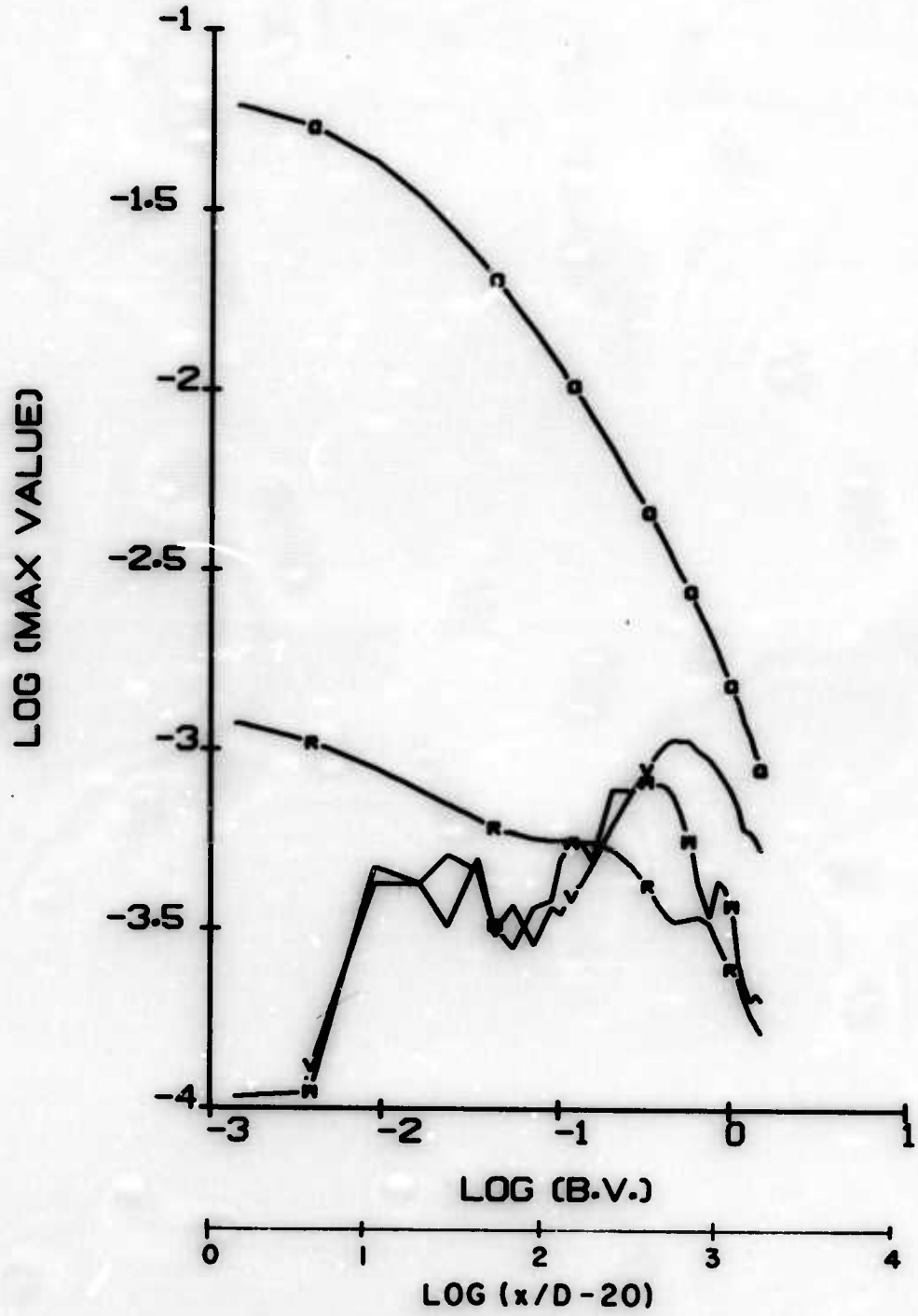


Figure 7. Maximum values of $q$, $\hat{\rho}$, $v$ and $w$ as a function of time after generation. (Initial conditions - Fr = 228., $q_m^2 = .00456$, $v = w = 0$ $\hat{\rho}_m = 1.$) Equivalent distance behind a Naudascher body is also indicated.

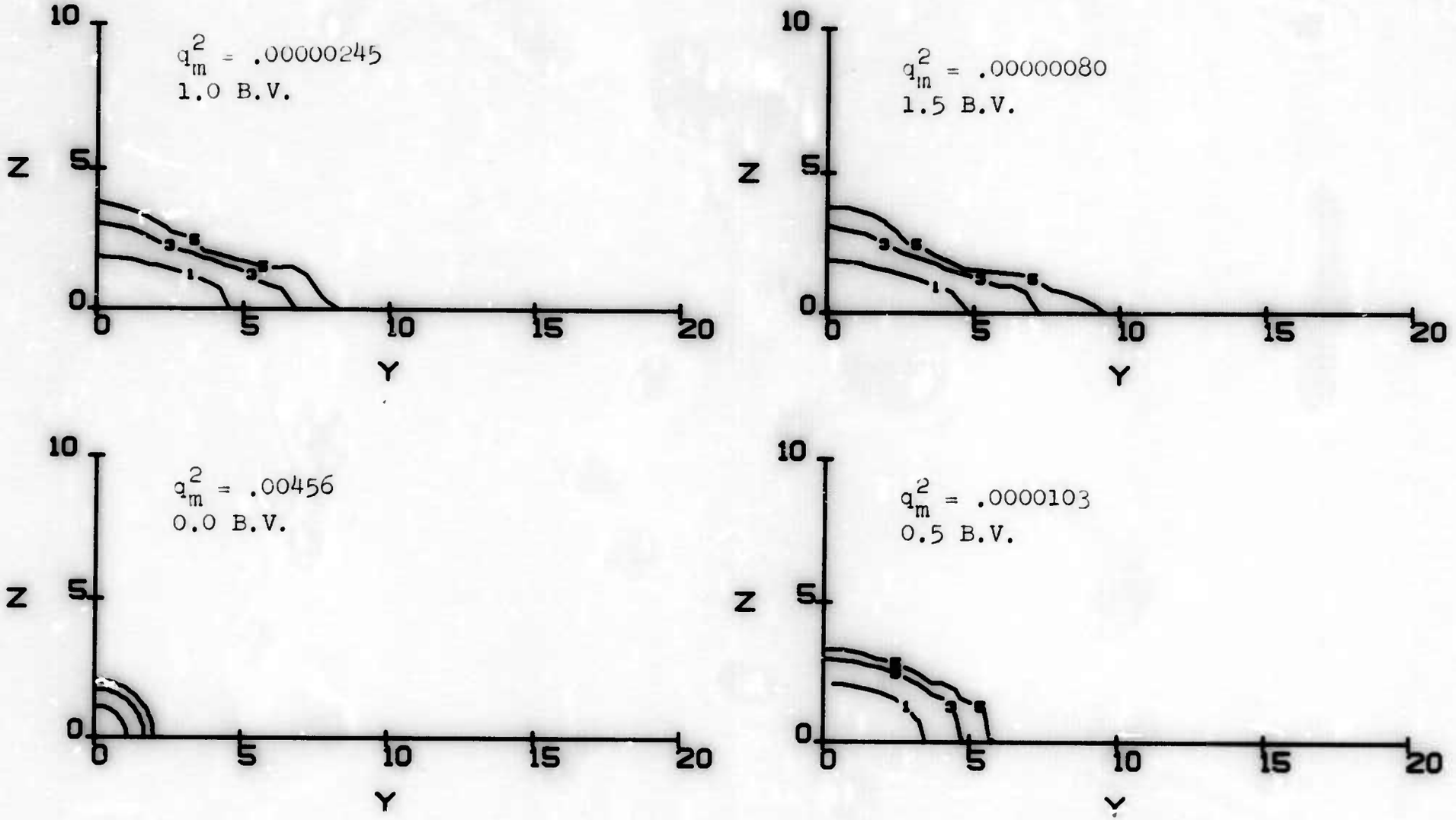


Figure 8. Contours of constant turbulent kinetic energy at different times after generation for the same conditions as Fig. 7. Contours for $q^2/q_m^2$ as denoted in Fig. 3.

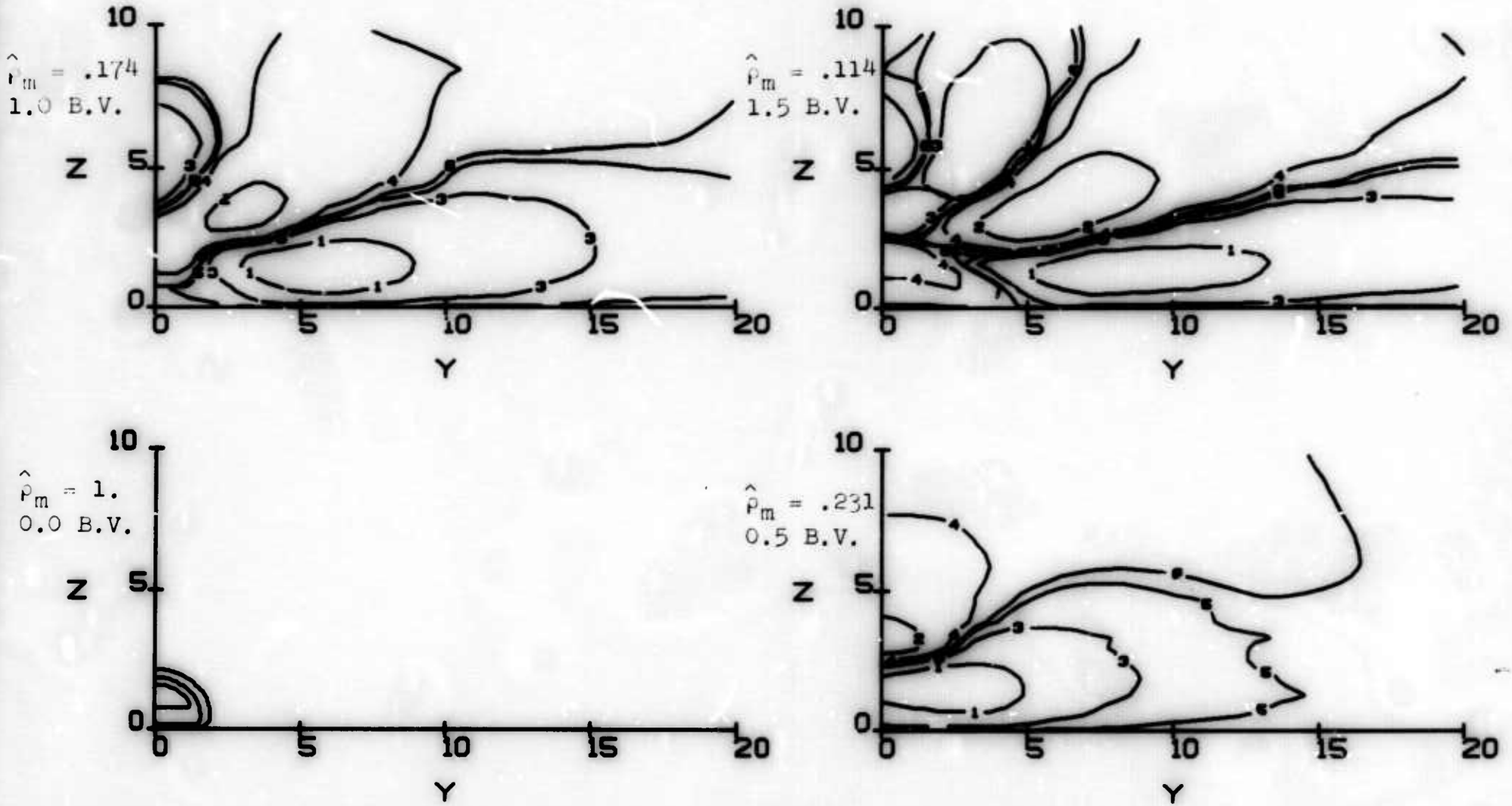


Figure 9. Contours of constant $\hat{\rho}$ at different times after generation for the same conditions as Fig. 7. Contours for $\hat{\rho}/\hat{\rho}_m$ as denoted in Fig. 3.

$\psi_m$ = .000440
1.5 B.V.

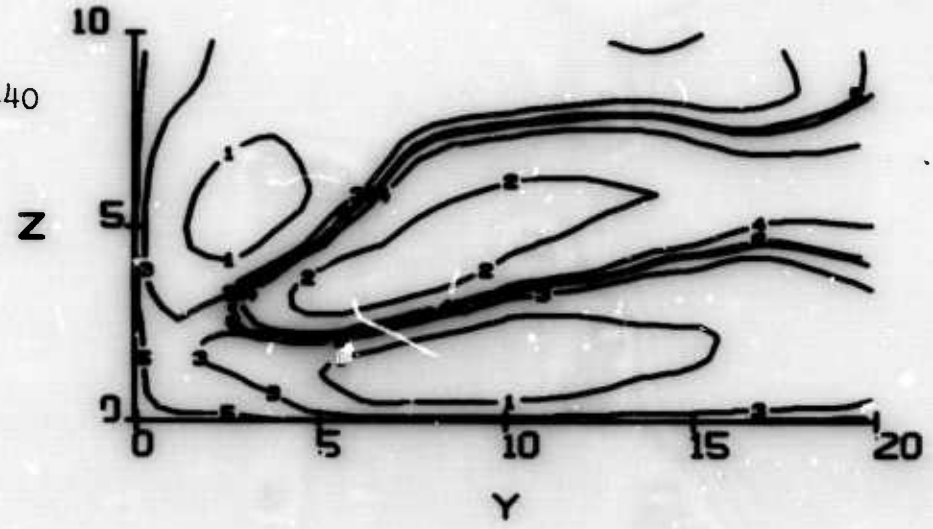


$\psi_m$ = .000708
1.0 B.V.

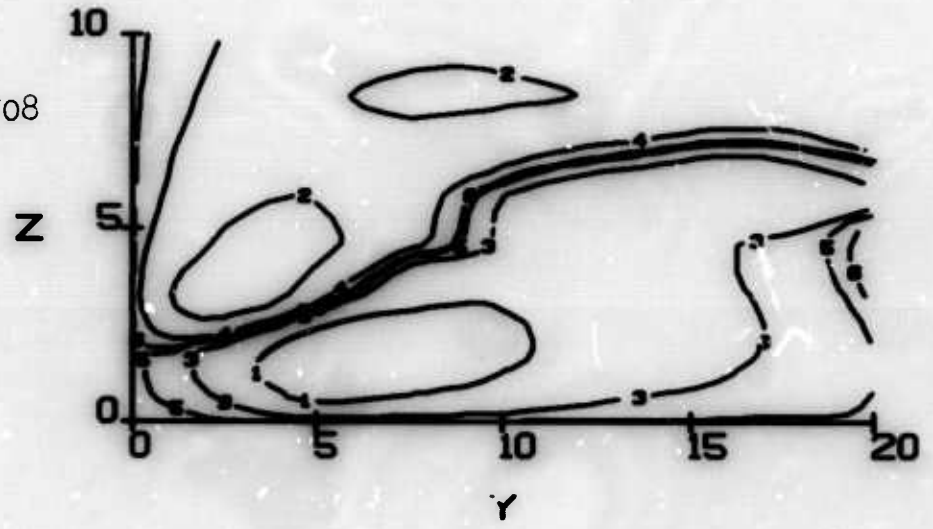


$\psi_m$ = .00128
0.5 B.V.

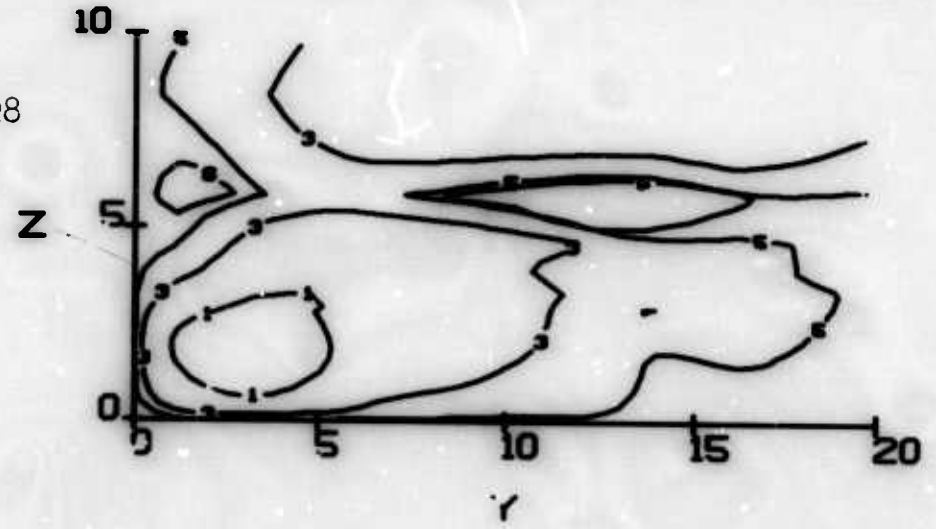


Figure 10. Normalized streamline patterns at different times after generation for the same conditions as Fig. 7. Contour notation for $\psi/\psi_m$ as in Fig. 3.

and the streamline patterns of the radiating waves at 0.0, 0.5, 1.0 and 1.5 B.V. periods after the wake generation.

When the stratification is increased the picture changes as seen in Figs. 11 to 14. Stratification becomes important a shorter distance behind the body, before the wake has grown to as large a radius as previously, and the strength of the streamline patterns produced by the collapse is increased. As a function of $x/D$, $q$ and $\hat{\rho}$ are the same for both runs until $x/D = 67$ ($\approx$ 0.1 B.V. on Fig. 11) at which point the stronger stratification forces $\hat{\rho}$ and $q$ to be decreased at a faster rate as $v$ and $w$ increase. In the region of the principal collapse (0.1 to 1 B.V.) $v$ and $w$ scale fairly closely with $N$, as seen in Figs. 7 and 11, and the streamline patterns are quite similar as seen in Figs. 10 and 14.

When the initial Richardson number is decreased by increasing the intensity of the turbulence, the results shown in Figs. 15 to 18 are obtained. The influence of stratification is delayed until the potential energy can build to a larger value. Consequently, a stronger streamline pattern is generated by the collapse although its occurrence is delayed further downstream.

The maximum potential energy per unit length of the wake occurs when the local Richardson number is of order one. Figure 19 shows how this maximum value varies as a function of the initial Richardson number over the range of initial Richardson numbers expected to be of interest for a submarine ($10^{-4} < Ri < 1$) when the initial distributions of density and turbulence are held constant. Sensitivity to variations in the distribution of the initial turbulence have not been computed but it is expected that these would have little influence on the dependence shown in Fig. 19 as long as the initial kinetic energy was fixed. The results are sensitive to variations in the initial ratio of potential to kinetic energy. Two curves obtained by starting with different initial density profiles are included on this curve to demonstrate this variation. As long as $Ri_o$ is small enough, the initial density distribution is unimportant

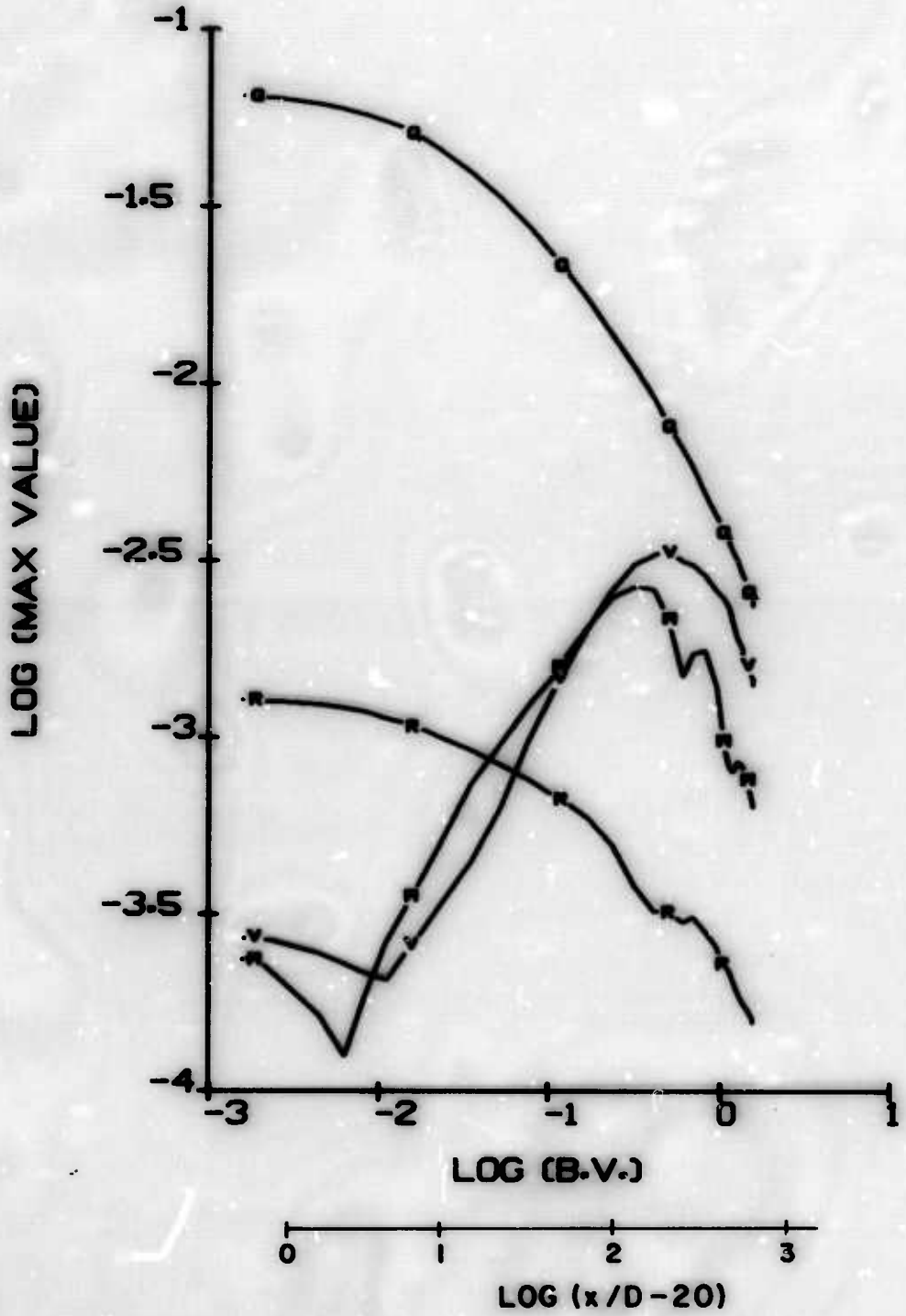


Figure 11. Maximum values of q , $\hat{\rho}$ , v and w as a function of time after generation. Initial conditions are the same as Fig. 7 except Fr is decreased by $\sqrt{10}$.

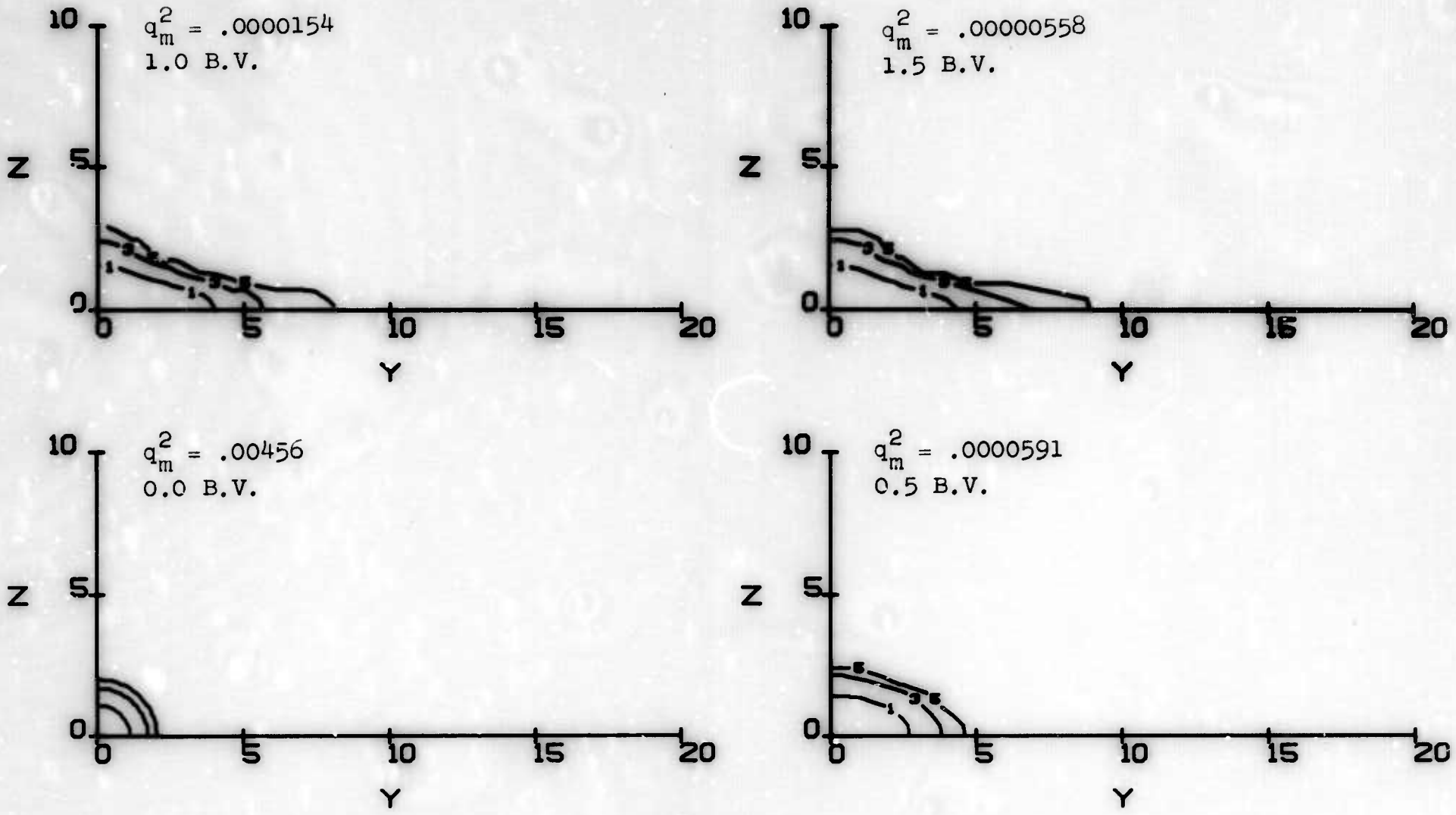


Figure 12. Contours of constant turbulent kinetic energy at different times after the generation for the same conditions as Fig. 11. Contour notation per Fig. 3.

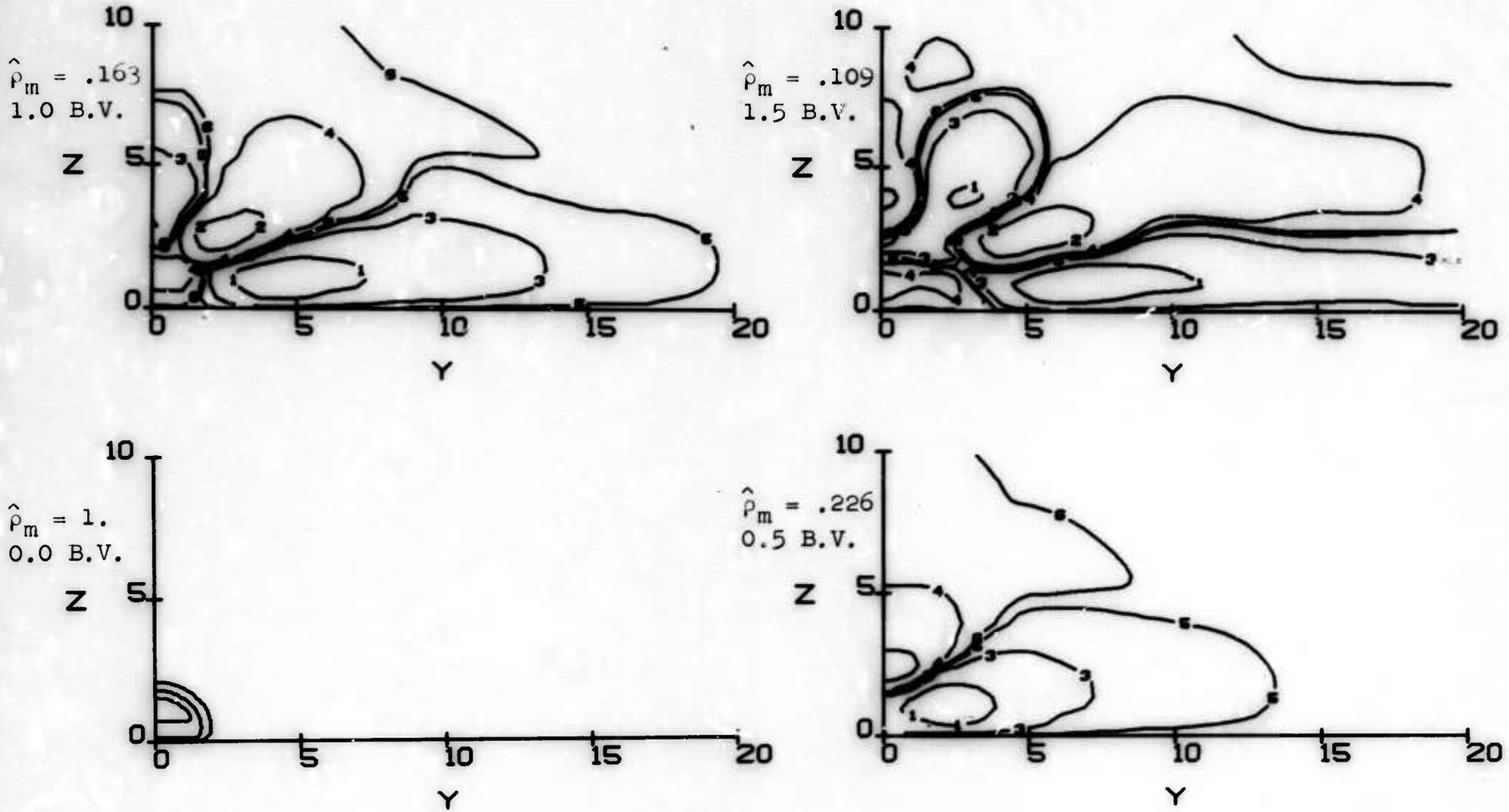


Figure 13. Contours of constant $\hat{\rho}$ at different times after generation for the same conditions as Fig. 11. Contour notation per Fig. 3.

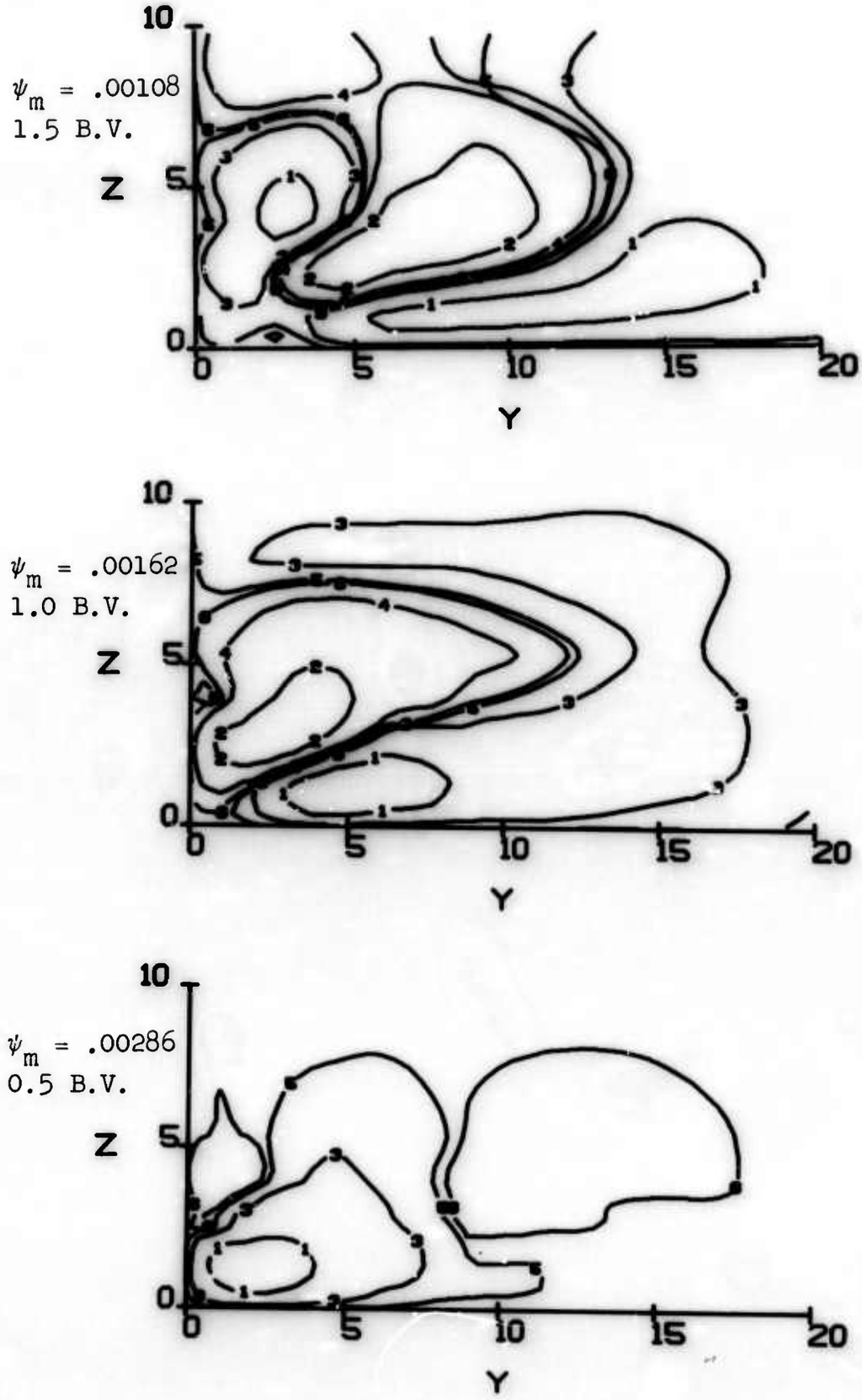


Figure 14. Normalized streamline patterns at different times after generation for the same conditions as Fig. 11. Contour notation per Fig. 3.

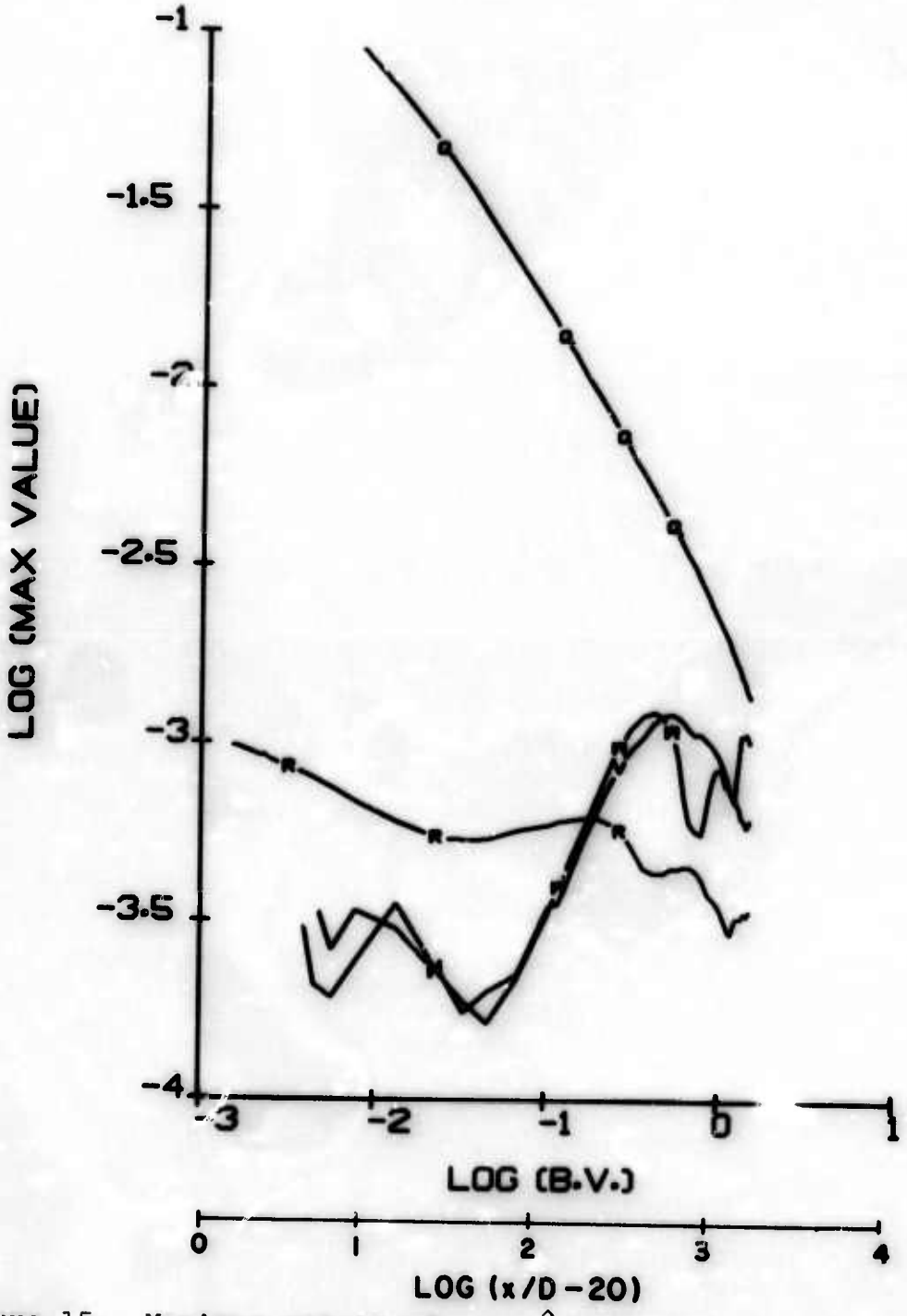


Figure 15. Maximum values of $q$, $\hat{\rho}$, $v$ and $w$ as a function of time after generation. Initial conditions are the same as Fig. 7 except $q_m^2$ is increased by ten.

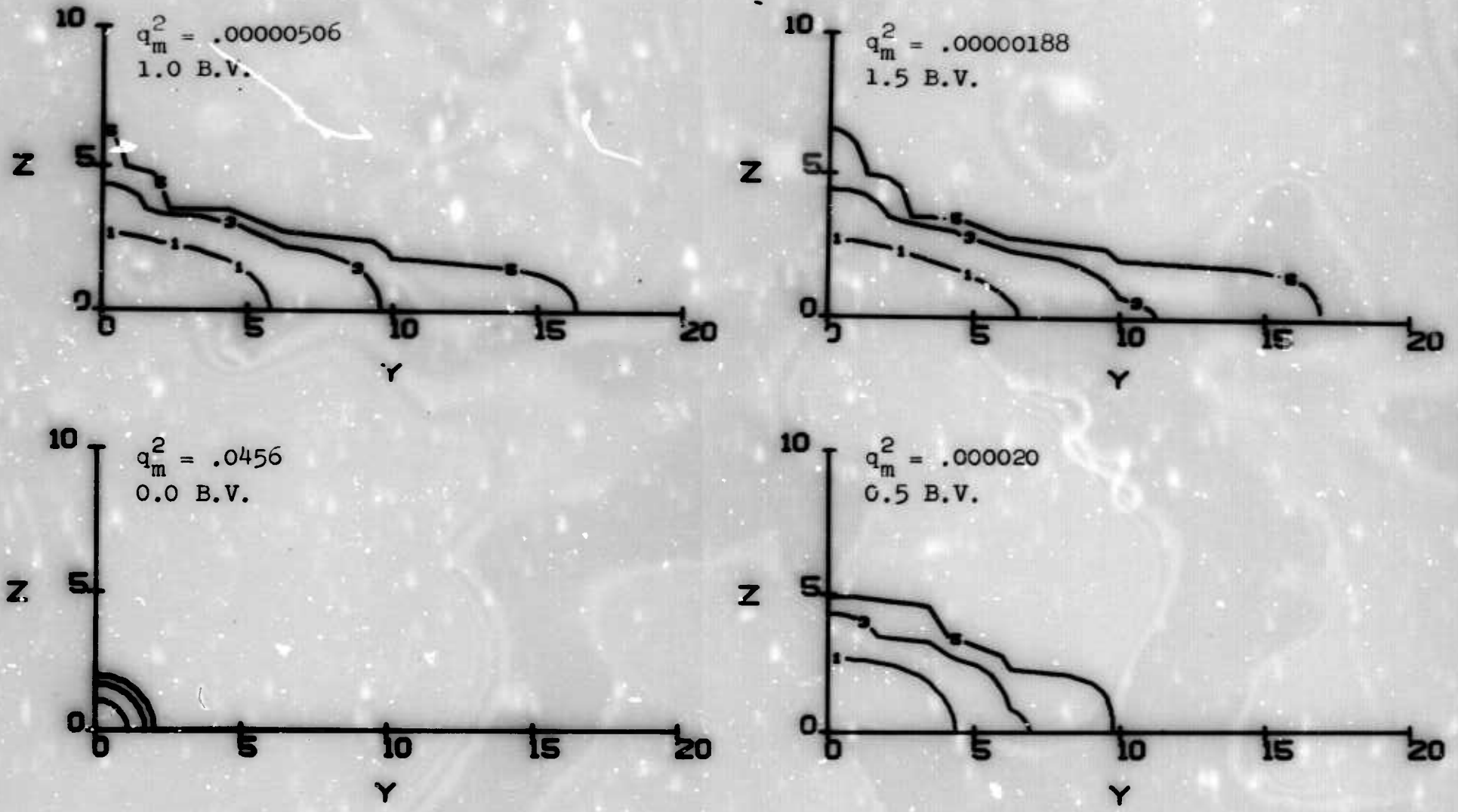


Figure 16. Contours of constant $q^2$ at different times after generation for the same condition as Fig. 15. Contour notation per Fig. 3.

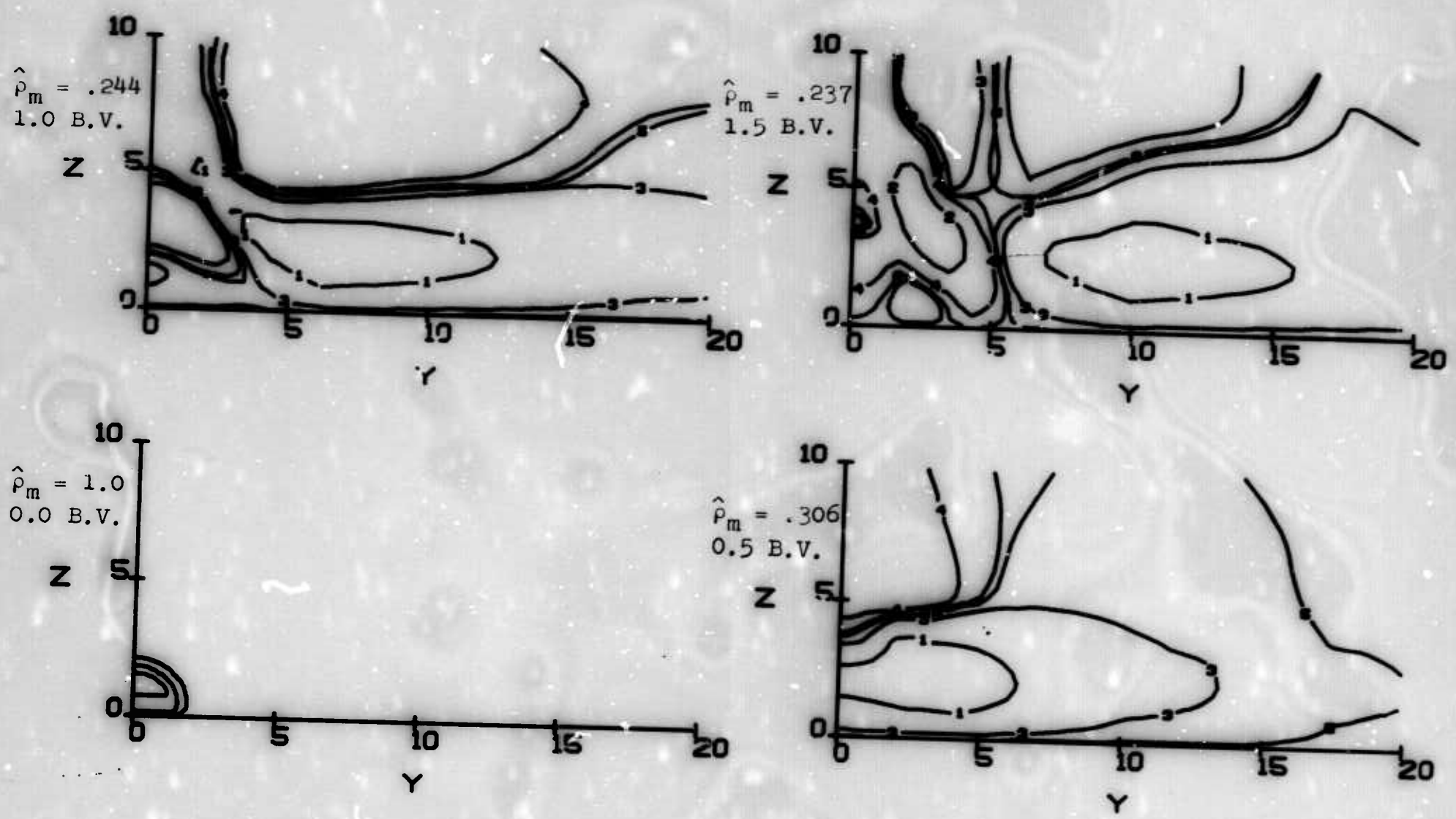


Figure 17. Contours of constant $\hat{\rho}$ at different times after generation for the same conditions as Fig. 15. Contour notation per Fig. 3.

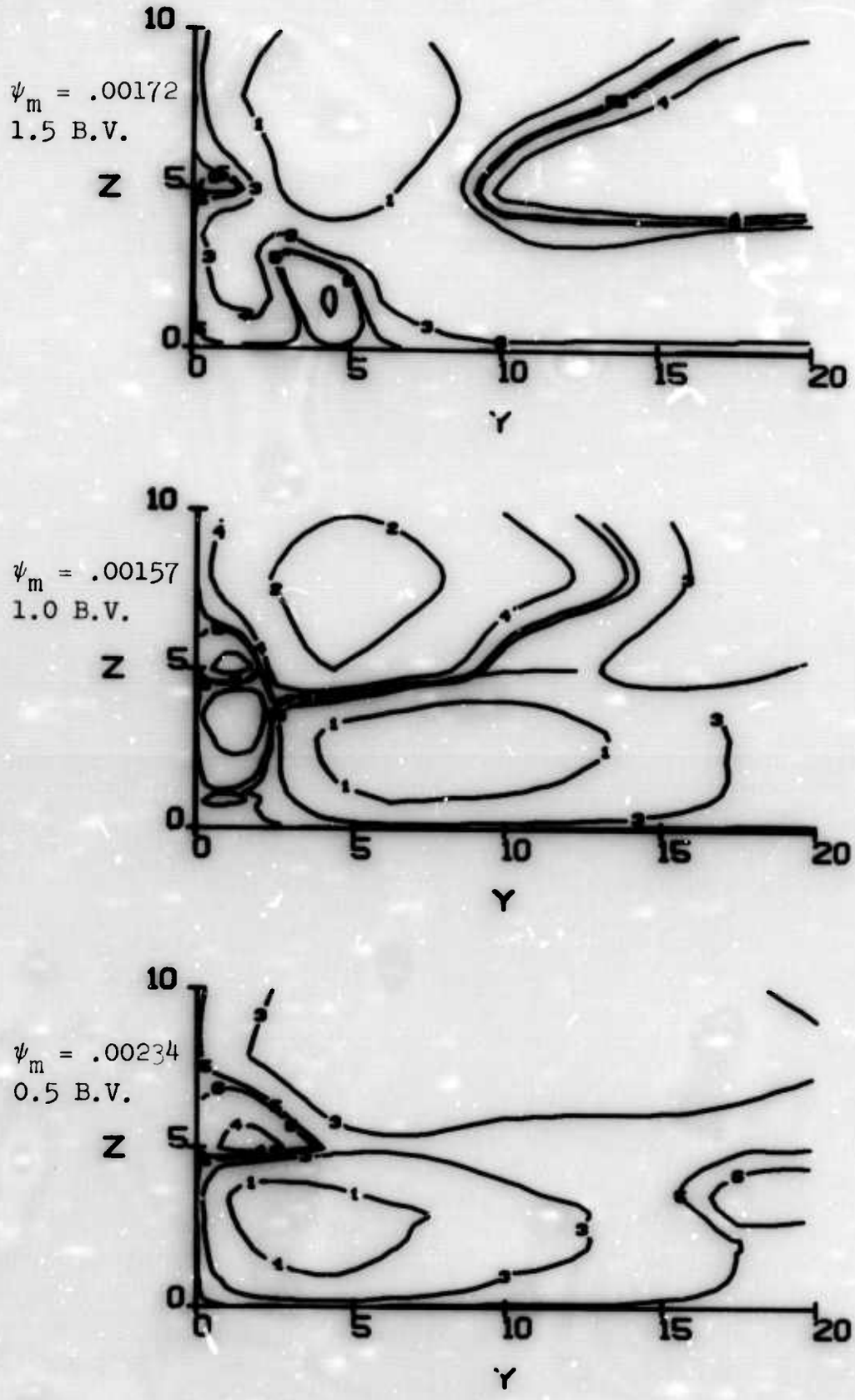


Figure 18. Normalized streamline patterns at different times after generation for the same conditions as Fig. 15. Contour notation per Fig. 3.

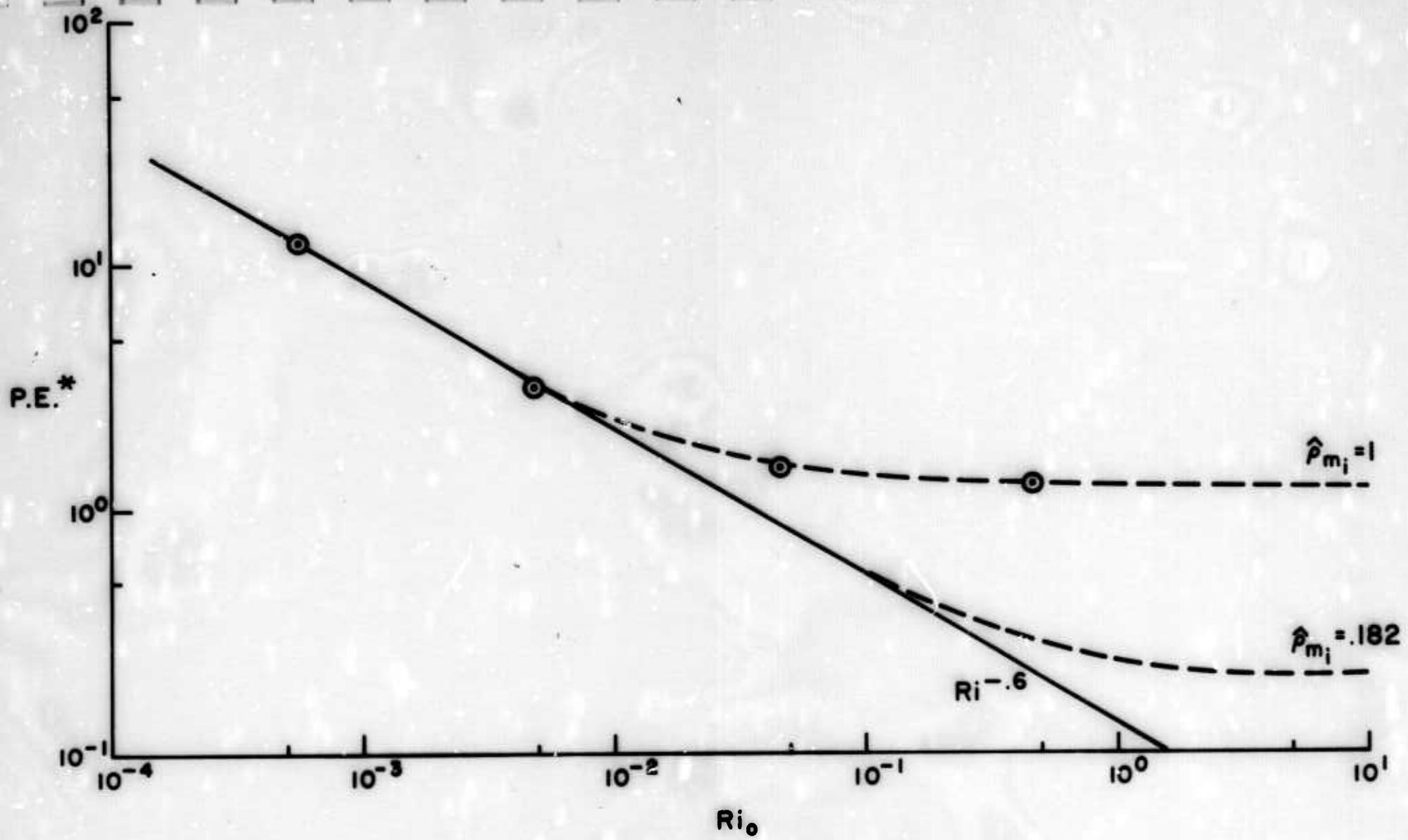


Figure 19. Maximum potential energy per unit length at any position behind the body as a function of initial Richardson number $Ri_o = r_i^2 N^2/q_m^2$ for two different values of initial $\hat{\rho}_m$ . P. E.* = $\left[\int_{-\infty}^{+\infty}\int_{-\infty}^{+\infty} \hat{\rho} z \, dydz\right]_m$ .

since the wake will continue to grow and develop its appropriate density distribution prior to collapse. When $Ri_o \geq 1$, collapse is imminent and the initial density distribution is a dominant factor. Since in this case the initial potential energy is the maximum value of potential energy, it is independent of $Ri_o$. The limiting asymptote for zero initial potential energy varies approximately with the -0.6 power of the initial Richardson number.

A summary curve showing the distortion of the wake as a function of time after generation is presented in Fig. 20 for several of the points on Fig. 19. The experimental variation as reported by Schooley and Stewart (Ref. 1) is also included. A detailed match of Schooley - Stewart's run has not been made yet since their initial $Ri \approx 0.1$, where it is necessary to also know the initial density distribution in the wake. It appears that a reasonable match could be made since their results fall between the $Ri = 0.0465$ and 0.465 model results.

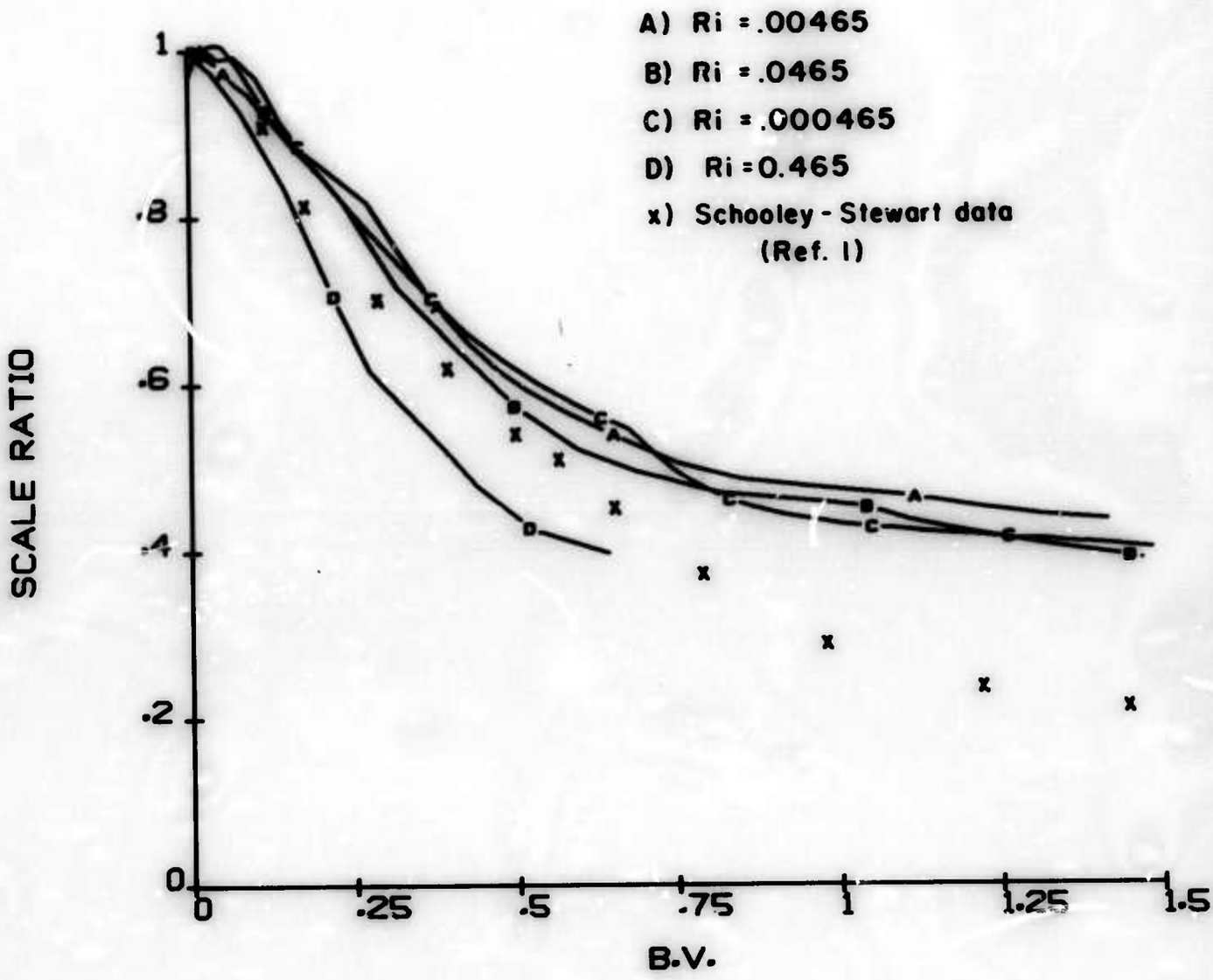


Figure 20. Wake distortion as a function of time for the four different points indicated on Fig. 19.

# 5. CONCLUSIONS AND FUTURE PLANS

We have created a computer model for the calculation of the development of a turbulent wake behind a submarine in a stratified ocean. The model results have been shown to be valid in several limiting cases. In the limit of vanishing stratification, it agrees with Naudascher's wake data in a homogeneous fluid; in the limit of starting with a uniformly mixed region in a strongly stratified fluid, it agrees with the observations of Wu; and in the limit of a small perturbation to the ambient linear density gradient and vanishing turbulence, it agrees with the analytical solution of Hartman and Lewis.

A detailed sensitivity study has not been made but the influences of some of the major parameters have been demonstrated by running a few typical cases. The influence of increasing the initial potential energy by increasing the degree of mixing is to advance the time of collapse and increase the strength of collapse unless the initial Richardson number is very much smaller than one, in which case there is no effect. Increasing the initial kinetic energy delays the time of collapse and increases the strength of collapse unless the initial Richardson number is much larger than one, in which case there is no effect. Increasing the Brunt-Väisälä frequency of the fluid always advances and strengthens the collapse.

We are currently in the process of conducting a much more complete investigation of the sensitivity of the wake-generated internal waves on initial conditions. This should include the influence of initial turbulence level, scale and distribution; of initial velocity distribution including asymmetrical swirl distributions; and of vertical, horizontal, or angular momentum as well as axial momentum. The completion of such an investigation will require that our model be generalized to include a turbulent scale equation and to compute all three momentum equations simultaneously.

We also recommend that experimental laboratory data be chosen by the contract monitor so that detailed comparisons between our model predictions and observations can be made for a stratified wake similar to that expected behind a submarine.

# 6. REFERENCES


1. Schooley, A. H. and R. W. Stewart: "Experiments with a Self-Propelled Body Submerged in a Fluid with a Vertical Density Gradient," J. Fluid Mechanics, 15, 1963, pp. 83-96.

2. Schooley, A. H.: "Wake Collapse in a Stratified Fluid," Science, 157, 1967, pp. 421-423.

3. Wu, J.: "Mixed Region with Internal Wave Generation in a Density-Stratified Medium," J. Fluid Mechanics, 35, 1969, pp. 531-544.

4. Wessel, W. R.: "Numerical Study of the Collapse of a Perturbation in an Infinite Density Stratified Fluid," Phys. Fluids, Supplement II, 1969, pp. 171-176.

5. Hartman, R. J. and H. W. Lewis: "Wake Collapse in a Stratified Fluid: Linear Treatment," J. Fluid Mech., 51, 1972, pp. 613-618.

6. Young, J. A. and C. W. Hirt: "Numerical Calculation of Internal Wave Motions," J. Fluid Mech. 56, 1972, pp. 265-276.

7. Mei, C. C.: "Collapse of a Homogeneous Fluid Mass in a Stratified Fluid," 12th Int. Congr. Appl. Mech., Springer Press, (1969), pp. 321-330.

8. Merritt, G. E.: "Wake Growth and Collapse in a Stratified Flow," AIAA Paper No. 73-108, January 1973.

9. Ko, D. R. S.: "A Phenomenological Model for the Momentumless Turbulent Wake in a Stratified Medium," TRW Report 20086-6007-RU-00, April 1973.

10. Dugan, J. P., A. C. Warn-Varnas and S. A. Piacsek: "Numerical Model for Mixed Region Collapse in a Stratified Fluid," NRL Memorandum Report 2597, June 1973.

11. Donaldson, Coleman, duP.: "Construction of a Dynamic Model of the Production of Atmospheric Turbulence and the Dispersal of Atmospheric Pollutants," American Meteorological Society Workshop in Micrometeorology, (D. A. Haugen, editor) Science Press, (1973), pp. 313-392.

12. Lewellen, W. S., M. Teske, and Coleman duP. Donaldson: "Application of Turbulence Model Equations to Axisymmetric Wakes," A.R.A.P. Report No. 191, February 1973.

13. Lewellen, W. S. and M. Teske: "Prediction of the Monin-Obukhov Similarity Functions from an Invariant Model of Turbulence," J. Atmospheric Sciences 30, 1973, pp. 1340-1345.

14. Mellor, G. L. and H. J. Herring: "A Survey of the Mean Turbulent Field Closure Models," AIAA J. 11, No. 5, 1973, pp. 590-599.

15. Naudascher, E.: "Flow in the Wake of Self-Propelled Bodies and Related Sources of Turbulence," J. Fluid Mechanics 22, 1965, pp. 625-656.

16. Gran, R. L.: "An Experiment on the Wake of a Slender Propeller-Driven Body," TRW Report 20086-6006-RU-00, June 1973.

17. Roache, P. J.: Computational Fluid Dynamics, Hermosa Publishers (1972).

18. Carnahan, B., H. A. Luther, and J. O. Wilkes: Applied Numerical Methods, Wiley Publishers (1969), pp. 452-453.